Cell Reports

Article

MAFB in macrophages regulates cold-induced neuronal density in brown adipose tissue

Graphical abstract

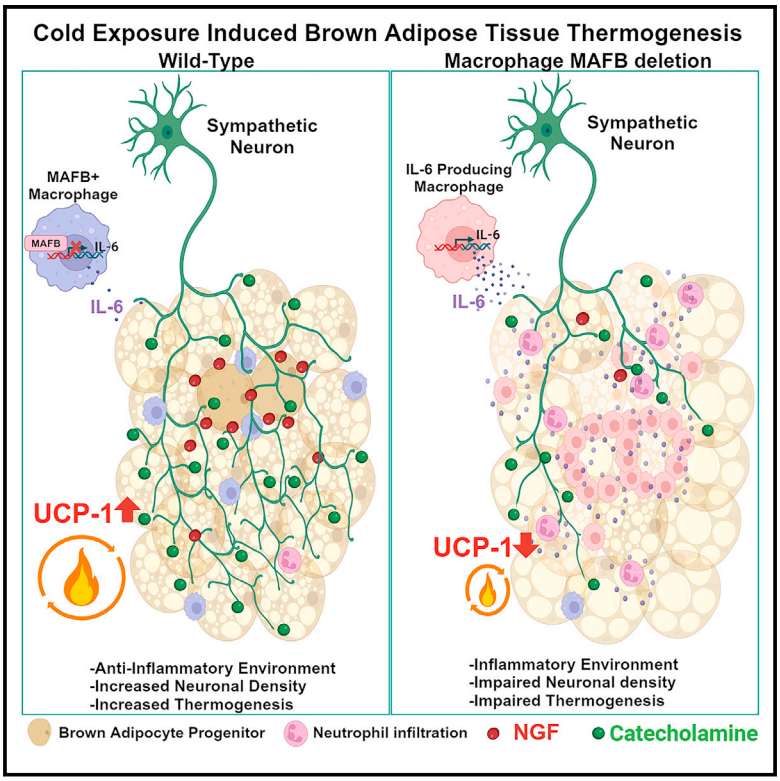

Highlights

- Macrophage MAFB deficiency impairs cold-induced BAT thermogenesis
- MAFB loss reduces BAT sympathetic neuron density in the cold
- MAFB represses macrophage IL-6 expression via promoter binding
- MAFB deficiency in macrophages induces inflammatory environment in BAT

Authors

Manoj Kumar Yadav, Megumi Ishida, Natalia Gogoleva, ..., Evaristus C. Mbanefo, Satoru Takahashi, Michito Hamada

Correspondence

satoruta@md.tsukuba.ac.jp (S.T.), hamamichi@md.tsukuba.ac.jp (M.H.)

In brief

Yadav et al. elucidates the role of the transcription factor MAFB in regulating brown adipose tissue (BAT) thermogenesis. They demonstrate that MAFB deficiency in macrophages decreases the neuronal density and thermogenesis of BAT in response to cold, due to an inflammatory state caused by an increase in IL-6, with accumulation of macrophages and granulocytes.

Yadav et al., 2024, Cell Reports *43*, 113978
April 23, 2024
https://doi.org/10.1016/j.celrep.2024.113978

CellPress

Cell Reports

CellPress
OPEN ACCESS

Article

MAFB in macrophages regulates cold-induced neuronal density in brown adipose tissue

Manoj Kumar Yadav,[1,2,3] Megumi Ishida,[1] Natalia Gogoleva,[1,2] Ching-Wei Liao,[1,2] Filiani Natalia Salim,[4] Maho Kanai,[1,2] Akihiro Kuno,[1] Takuto Hayashi,[1,5] Zeynab Javanfekr Shahri,[1,2] Kaushalya Kulathunga,[1,2] Omar Samir,[6,7,8] Wenxin Lyu,[2,9,10] Olivia Olivia,[11] Evaristus C. Mbanefo,[3] Satoru Takahashi,[1,12,13,14,*] and Michito Hamada[1,12,15,*]

[1]Department of Anatomy and Embryology, Faculty of Medicine, University of Tsukuba, Tsukuba 305-8575, Japan
[2]Ph.D. Program in Human Biology, School of Integrative and Global Majors, University of Tsukuba, Tsukuba 305-8575, Japan
[3]National Institutes of Health, Bethesda, MD 20892, USA
[4]Centre for Medical Science and Technology and Healthcare Equity, Parahyangan Catholic University, Bandung 40141, Indonesia
[5]Graduate School of Comprehensive Human Sciences, University of Tsukuba, Tsukuba 305-8575, Japan
[6]Department of Pathology, Faculty of Veterinary Medicine, Mansoura University, Mansoura 35516, Egypt
[7]Department of Medicine, Harvard Medical School, Boston, MA 02115, USA
[8]Jeff and Penny Vinik Center for Allergic Disease Research, Division of Rheumatology, Immunology, and Allergy, Brigham and Women's Hospital, Boston, MA 02115, USA
[9]Department of Immunology, Faculty of Medicine, University of Tsukuba, Tsukuba 305-8575, Japan
[10]Department of Immunology and Microbiology, LEO Foundation Skin Immunology Research Center, University of Copenhagen, 2200 Copenhagen, Denmark
[11]Faculty of Medicine, Universitas Padjadjaran, Sumedang 45363, Indonesia
[12]Laboratory Animal Resource Center (LARC), Faculty of Medicine, University of Tsukuba, Tsukuba 305-8575, Japan
[13]International Institute for Integrative Sleep Medicine (WPI-IIIS), University of Tsukuba, Tsukuba 305-8575, Japan
[14]Life Science Center for Survival Dynamics, Tsukuba Advanced Research Alliance, University of Tsukuba, Tsukuba 305-8575, Japan
[15]Lead contact
*Correspondence: satoruta@md.tsukuba.ac.jp (S.T.), hamamichi@md.tsukuba.ac.jp (M.H.)
https://doi.org/10.1016/j.celrep.2024.113978

SUMMARY

Transcription factor MAFB regulates various homeostatic functions of macrophages. This study explores the role of MAFB in brown adipose tissue (BAT) thermogenesis using macrophage-specific *Mafb*-deficient (*Mafb*$^{f/f}$::LysM-Cre) mice. We find that *Mafb* deficiency in macrophages reduces thermogenesis, energy expenditure, and sympathetic neuron (SN) density in BAT under cold conditions. This phenotype features a proinflammatory environment that is characterized by macrophage/granulocyte accumulation, increases in interleukin-6 (IL-6) production, and IL-6 *trans*-signaling, which lead to decreases in nerve growth factor (NGF) expression and reduction in SN density in BAT. We confirm MAFB regulation of IL-6 expression using luciferase readout driven by IL-6 promoter in RAW-264.7 macrophage cell lines. Immunohistochemistry shows clustered organization of NGF-producing cells in BAT, which are primarily TRPV1^{+} vascular smooth muscle cells, as additionally shown using single-cell RNA sequencing and RT-qPCR of the stromal vascular fraction. Treating *Mafb*$^{f/f}$::LysM-Cre mice with anti-IL-6 receptor antibody rescues SN density, body temperature, and energy expenditure.

INTRODUCTION

Brown adipose tissue (BAT) is an important organ for cold-induced thermogenesis. During cold exposure, nonshivering heat production is induced via sympathetic neuron (SN) signaling from the hypothalamic preoptical area cold-specific neurons.[1] Previous studies have shown that prolonged cold acclimatization in mice alters sympathetic neuronal density in adipose tissue via the upregulation of uncoupling protein-1 (UCP-1) expression in BAT.[2] UCP-1 is responsible for BAT thermogenic function via the β3-adrenergic receptor signal sensing from SN-derived norepinephrine.[3] Other reports have shown that macrophages regulate BAT cold-induced thermogenesis by other functional pathways. Mice having macrophage-specific deletion of the methyl-CpG binding protein 2 (*MECP2*) gene exhibit reduced sympathetic innervation of BAT due to increased plexin A4, which regulates the repulsion of sympathetic axons.[4] The M2 polarization of macrophages was also shown to promote the activation of brown adipocytes following cold induction.[5–7] In addition, crosstalk between adipose tissue macrophages and neurons has been reported, showing that SN-associated macrophages mediate the clearance of norepinephrine and inhibit the energy expenditure of BAT and white adipose tissue (WAT).[8] Other innervation-regulating factors have been reported to be expressed in BAT such as nerve growth factor (NGF),[9] calsyntenin 3b,[10] and CREB-regulated

transcription coactivator 3.[11] However, detailed molecular mechanisms have not been elucidated.

Musculoaponeurotic fibrosarcoma oncogene homolog B (MAFB) is a basic-leucine zipper transcription factor that belongs to the large MAF oncogene family and binds to a specific DNA sequence called Maf-recognition elements in the regulatory regions of target genes.[12] MAFB is specifically expressed in the macrophage lineage of hematopoietic cells.[13] Recent studies have shown that MAFB is essential for the various homeostatic functions of macrophages[14] and regulates the uptake of apoptotic cells by regulating the *C1q* genes.[15] MAFB expression in WAT macrophages affects adipocyte lipogenesis in high-fat diet (HFD)-fed mice.[16] It has a role in atherosclerosis progression in hyperlipidemic conditions and inhibits foam cell apoptosis.[17] These studies suggest that MAFB may be related to energy metabolism and homeostasis in adipose tissue under specific conditions. We hypothesized, therefore, that it may also play a previously unknown, key role in BAT metabolism.

In this study, we used macrophage-specific *Mafb* knockout (KO) mice (*Mafb*$^{f/f}$::LysM-Cre) to examine the activity of BAT in detail, under cold conditions, expanding the understanding of the transcriptional regulation of macrophages and the role of MAFB during macrophage-induced thermogenesis in BAT. We found that the loss of MAFB in macrophages decreased sympathetic neuronal density and lowered body temperature in *Mafb*$^{f/f}$::LysM-Cre mice compared to *Mafb*$^{f/f}$. These results suggest that MAFB is a key factor regulating body temperature and could be a therapeutic target for increasing the metabolism in BAT during thermogenesis.

RESULTS

Mafb expression in BAT increased upon cold exposure

To investigate the role of MAFB in BAT thermogenesis, we exposed C57BL/6J mice littermates to mild cold (8°C) on alternate days for 1 week, and the other group was maintained at standard laboratory temperature. We collected interscapular BAT (iBAT) samples for RT-qPCR and immunohistochemistry (IHC) analysis and found increased *Mafb* expression, *Ucp-1* levels, and MAC2^{+} (also known as galectin-3 [served as adipose tissue macrophage marker][18–20]) macrophages in cold-exposed mice (Figures 1A–1C). In addition, analysis of single-cell RNA sequencing data from BAT-stromal vascular fraction (BAT-SVF) lineage-positive sorted cells from mice exposed to cold for 4 days[21] showed an increase in MAFB^{+} macrophages (Figure 1D; Table S1), confirming the role of MAFB in cold acclimatization. Functional analysis of the MAFB^{+} versus MAFB^{-} macrophages in the BAT-SVF using Ingenuity Pathway Analysis showed downregulation of several inflammatory signaling pathways. These pathways include classical activation of macrophages (M1), neuroinflammation, interleukin-6 (IL-6), and oxidative stress signaling pathways compared to MAFB^{-} macrophages (Figure S1A). Conversely, MAFB^{+} macrophages demonstrate increased activation of anti-inflammatory pathways (Figure S1A). This suggests that the observed increase in MAFB^{+} macrophages during cold exposure has an anti-inflammatory role. Interestingly, norepinephrine (a sympathetic neurotransmitter released after cold sensation in BAT) treatment induced the expression of *Mafb* in an *in vitro* culture of bone marrow-derived macrophages (BMDMs) or thioglycolate-induced peritoneal-derived macrophages (Figures 1E and 1F). Moreover, β2 adrenergic receptors (ADRB2) for norepinephrine sensing were increased in macrophage-specific *Mafb*-deficient (*Mafb*$^{f/f}$::LysM-Cre) mice macrophages, possibly due to a compensatory mechanism (Figures S1B and S1C). This suggests that MAFB is possibly regulated by sympathetic stimuli in cold-acclimated mice BAT macrophages.

Susceptibility of mice with macrophage-specific *Mafb* deletion to cold-induced thermogenesis

To investigate the functional role of MAFB in BAT macrophages during cold acclimatization conditions, we followed a previously established protocol by Murano et al.[2] We subjected *Mafb*$^{f/f}$ and *Mafb*$^{f/f}$::LysM-Cre littermates to 10 days of continuous cold exposure or acute cold exposure after intermittent cold habituation. The *Mafb*$^{f/f}$::LysM-Cre mice group had lower rectal and skin temperatures than *Mafb*$^{f/f}$ mice only after exposure to cold conditions (Figures 2A–2C and S2A–C). Reduced body temperature could be attributed to reduced BAT thermogenic activity or muscle shivering. We confirmed BAT thermogenic activity in *Mafb*$^{f/f}$::LysM-Cre phenotype by injecting β3 agonists (CL-316243 disodium) into the mice after a 10-day cold exposure or room temperature exposure via indirect calorimetry. Cold-exposed *Mafb*$^{f/f}$::LysM-Cre mice administered with the drug had a decreased relative VO_{2max} compared with the *Mafb*$^{f/f}$ control mice group (Figure 2D), whereas there was no difference in relative VO_{2max} between the *Mafb*$^{f/f}$ control and *Mafb*$^{f/f}$::LysM-Cre maintained at room temperature (Figure S2D). In addition, we observed that the 10-day cold-exposed *Mafb*$^{f/f}$::LysM-Cre mice group had increased body weight compared to the *Mafb*$^{f/f}$ group while having similar food consumption (Figures 2E, 2F, and S2E–S2G). Furthermore, after a 10-day cold exposure followed by 1 day's rest at room temperature, indirect calorimetry showed differences in the respiratory quotient (RQ) without having significant differences in relative VO_{2max}. The *Mafb*$^{f/f}$::LysM-Cre mice had a higher RQ, suggesting less fat utilization for metabolism compared to the control *Mafb*$^{f/f}$ (Figures 2G and S2H). These results indicate that *Mafb*$^{f/f}$::LysM-Cre has reduced BAT metabolic activity and body temperature compared to *Mafb*$^{f/f}$ in cold environments, leading to increased body weight.

Inefficient thermogenic function of BAT in *Mafb*$^{f/f}$::*LysM-Cre* mice

Our phenotypical analysis showed that *Mafb*$^{f/f}$::LysM-Cre mice exhibited reduced heat production in cold environments; this reduction is likely due to impaired thermogenic function in BAT, which contributes a significant amount of heat production for maintaining the body temperature of rodents. To explore the role of MAFB in BAT thermogenesis, we used an inducible *Mafb* deletion mouse model, *Mafb*$^{f/f}$::Cag-Cre ERT2. In 8-week-old mice, we induced *Mafb* deletion with 5 consecutive tamoxifen injections and analyzed their BAT 7 days postinjection. RNA analysis revealed significant downregulation of *Mafb* and *Ucp1* expression in the iBAT of*Mafb*$^{f/f}$::Cag-Cre ERT2 mice compared to *Mafb*$^{f/f}$ littermate controls (Figure S3A), with complete suppression of *Mafb* expression in the iBAT of these mice (Figure S3A).

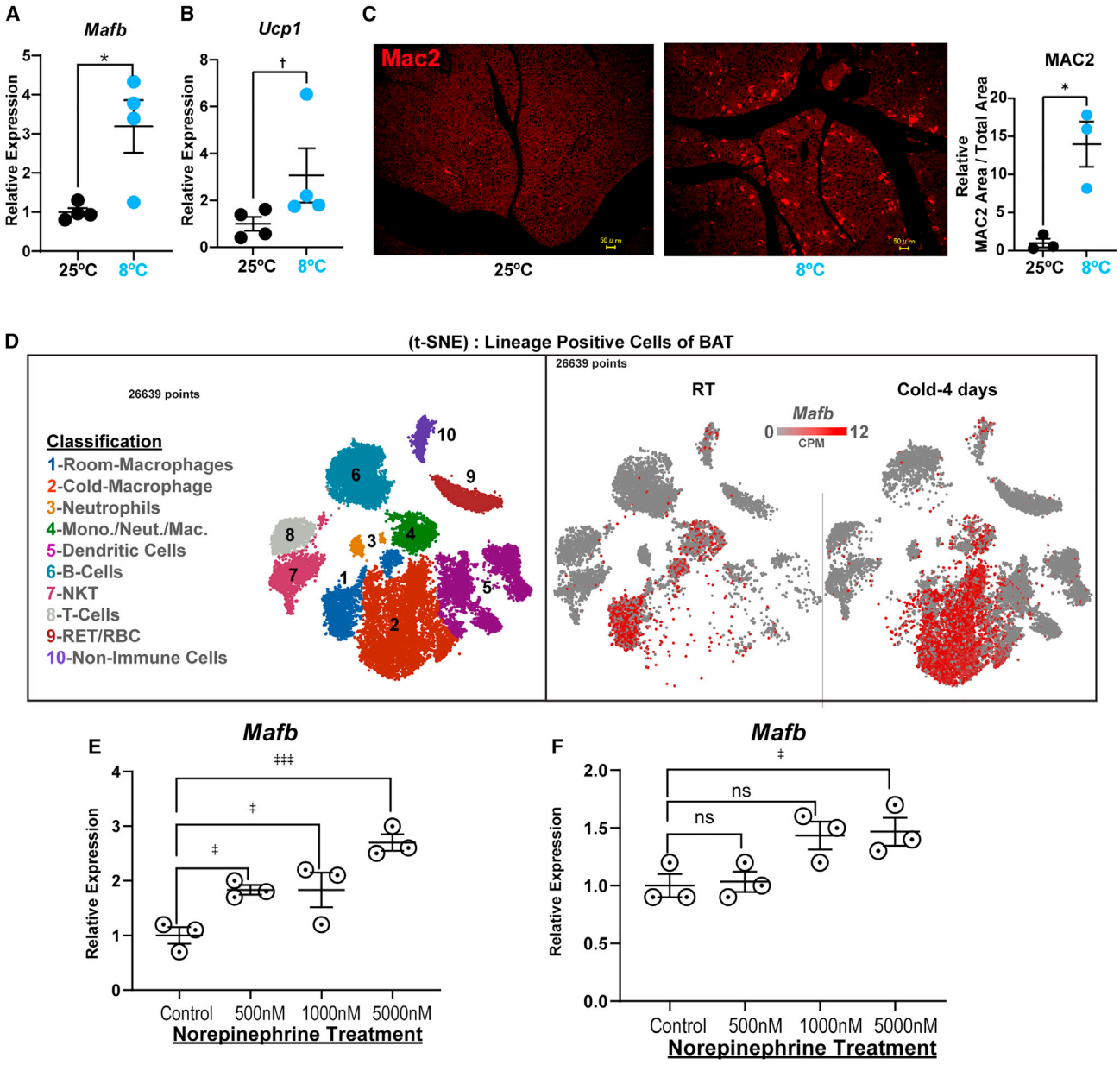

Figure 1. MAFB is increased in BAT after cold expression

Wild-type (C57BL/6J) mice were exposed at 8°C on alternate days for 8 h for cold acclimatization, followed by exposure to 8°C for up to 4 h. iBAT was collected and processed for RT-qPCR or IHC.

(A) RT-qPCR of *Mafb* (n = 4 per group).

(B) RT-qPCR of *Ucp1* (n = 4 per group).

(C) IHC of iBAT using MAC2 macrophage marker. scale bars, 50 μm.

(D) Single-cell RNA sequencing analysis of Database: GSE207706 data (Burl et al., 2022a[21]) of BAT SVF from control and cold-exposed mice, t-SNE plots for cell classification, and *Mafb* expression (n = 2).

(E) BMDM cultured from wild-type mice; on day six, the cells were treated in culture with norepinephrine (NE) for 12 h and RT-qPCR for *Mafb*.

(F) Thioglycolate-stimulated Peritoneal macrophages isolated from mice were cultured with NE treatment for 12 hours and RT-qPCR for *Mafb* performed(n = 4). Data presented as mean ± SEM. *$p < 0.05$, Welch's t test, †$p < 0.05$, Mann-Whitney test, ‡$p < 0.05$, ‡‡‡$p < 0.001$; 1-way ANOVA with least significant difference (LSD) test; ns, not significant.

Furthermore, we used *Mafb*$^{f/f}$::LysM-Cre for macrophage-specific *Mafb* deletion and *Mafb*$^{f/f}$::Adipoq-Cre for adipose tissue-specific *Mafb* deletion. Both models, along with their *Mafb*$^{f/f}$ littermate controls, were subjected to 10 days of continuous cold exposure. The iBAT of the *Mafb*$^{f/f}$::LysM-Cre BAT model showed a 35% decrease in *Mafb* expression and

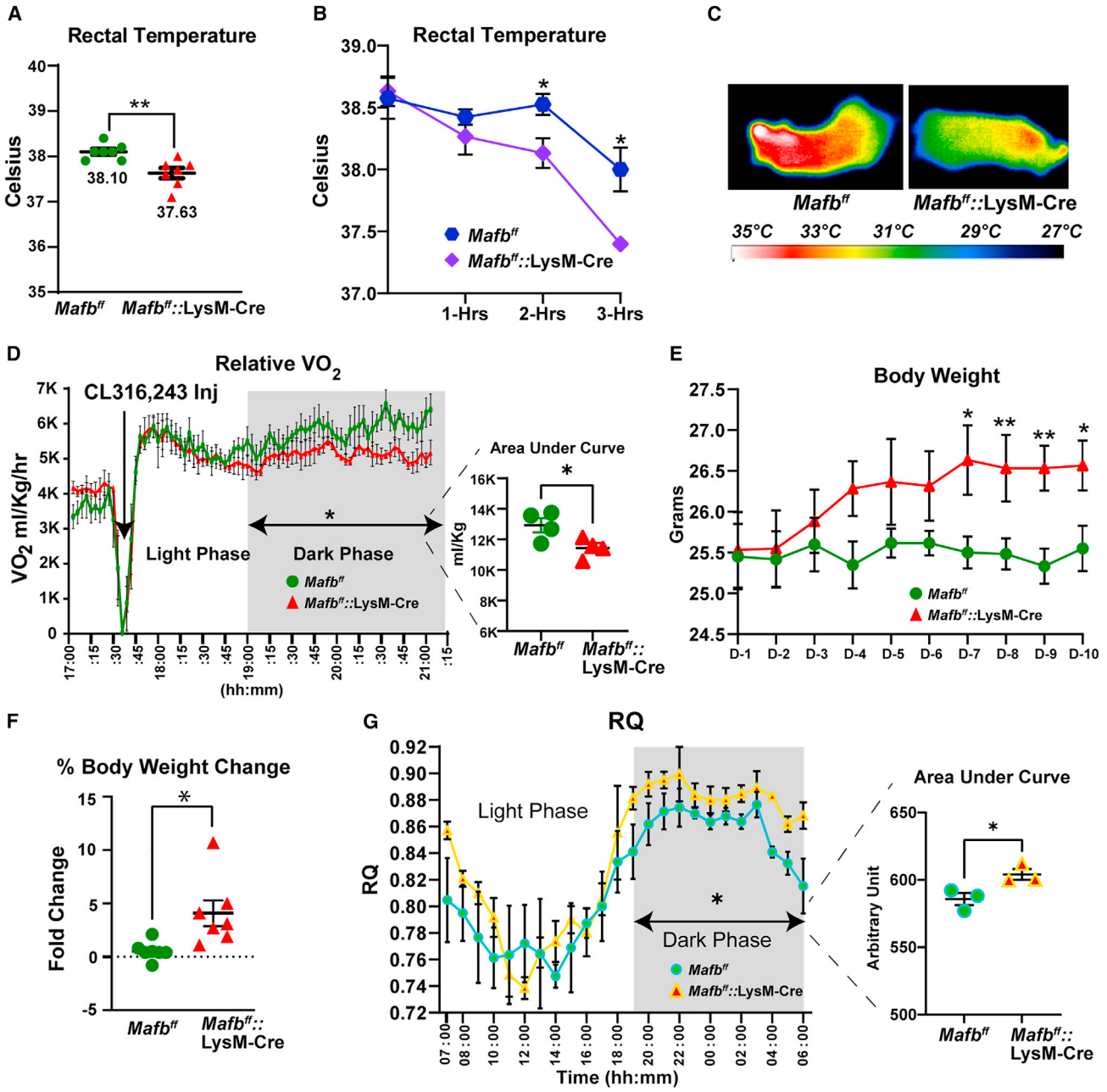

Figure 2. Body temperature and energy metabolism of *Mafb*$^{f/f}$::LysM-Cre are reduced following cold exposure

Littermates of *Mafb*$^{f/f}$ and *Mafb*$^{f/f}$::LysM-Cre mice were subjected to continuous cold for 10 days. The acute cold exposure, after intermittent cold acclimization, then mice were exposed at 8°C for up to 3 h.

(A) Rectal temperature after 10 days of exposure (n = 7 per group).

(B) Rectal temperature during a 3-h acute cold exposure at 8°C (*Mafb*$^{f/f}$ n = 4; *Mafb*$^{f/f}$::LysM-Cre; n = 3).

(C) Surface temperature measured after 10 days of cold exposure.

(D) Relative VO_2 on day 10 after β3 agonist injection (1 mg/kg of body weight); area under the curve quantified at right for dark phase (n = 4 per group).

(E) Body weight was monitored during 10 days of cold exposure(n = 6 per group).

(F) Percent body weight was calculated after the 10 days of cold exposure (n = 6 per group).

(G) Relative quotient (RQ; VCO_2/VO_2) measured after 10 days of cold exposure and 1 day of rest at room temperature (n = 4 per group).

Data are presented as mean ± SEM. *p < 0.05, **p < 0.01; Welch's t test.

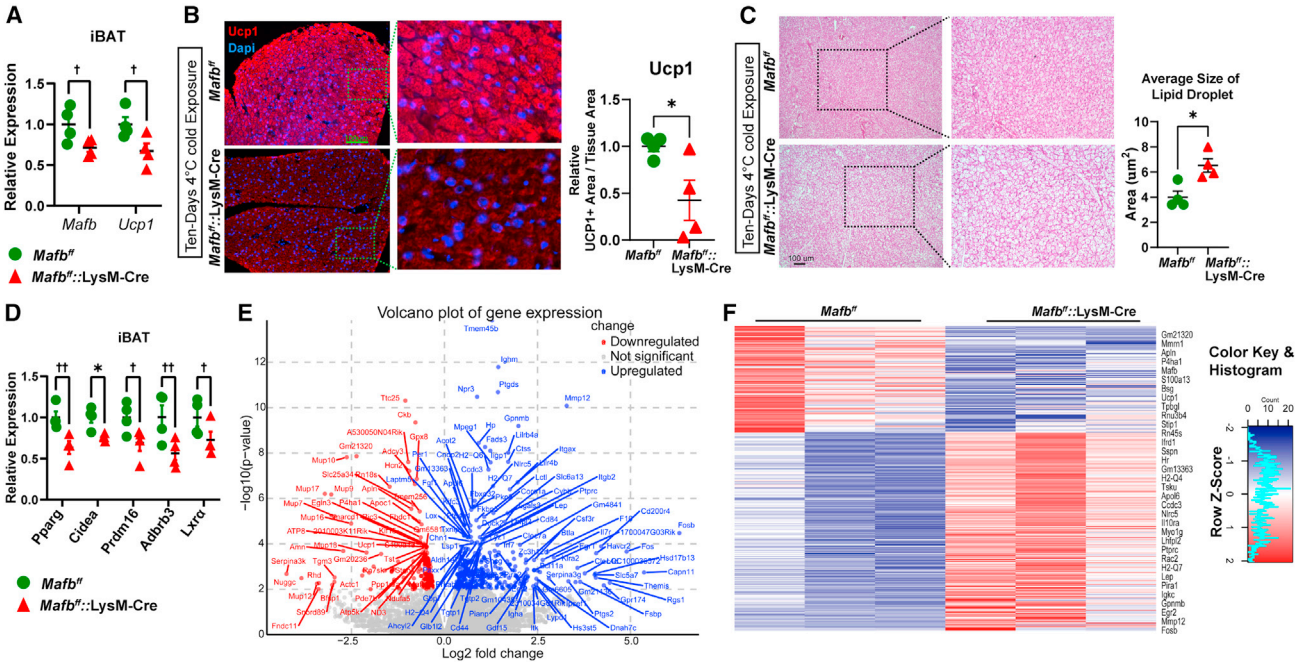

Figure 3. Inefficient BAT function in *Mafb*$^{f/f}$::LysM-Cre mice

Littermates of *Mafb*$^{f/f}$ and *Mafb*$^{f/f}$::LysM-Cre mice were exposed to cold for 10 days; iBAT was collected for histology, IHC, and RT-qPCR.

(A) *Mafb* and *Ucp1* mRNA expression (n = 4 for each group).

(B) IHC with anti-Ucp1 (red) and DAPI (blue), quantifying Ucp1$^+$ area/tissue area (n = 4 for each group). Scale bar, 100 μm.

(C) H&E staining of iBAT and lipid droplet size quantification (n = 4 for each group).

(D) BAT-specific gene mRNA expression (n = 4 for each group).

(E) Volcano plot differentially expressed genes following RNA sequencing in iBAT from mice exposed to 10 days of cold (n = 3 per group).

(F) Heatmap plot of differentially expressed genes following RNA sequencing in iBAT from mice exposed to 10 days of cold (n = 3 per group).

Data are presented as mean ± SEM. *p < 0.05, Welch's t test; †p < 0.05, ††p < 0.01; 2-way ANOVA with LSD Fisher test.

reduced *Ucp1* RNA levels compared to controls (Figure 3A). In contrast, the *Mafb*$^{f/f}$::Adipoq-Cre model exhibited a tendency to decrease in *Mafb* without affecting *Ucp1* levels (Figure S3B), suggesting that macrophage-specific MAFB expression significantly affects BAT thermogenesis, whereas adipocyte MAFB expression does not. To further clarify the LysM-Cre efficiency in the *Mafb*$^{f/f}$::LysM-Cre mice, we analyzed *Mafb* RNA in ependymal WAT (eWAT) and inguinal WAT (iWAT) after the 10 days of cold exposure, BMDM and peritoneal macrophages culture, and BAT's CD45$^+$CD11b$^+$Gr-1$^-$ macrophage populations. We observed a 98% reduction in *Mafb* RNA, indicating the high efficiency of LysM-Cre in deleting *Mafb* in macrophages (Figures S3C and S3D). *Ucp1* RNA levels in iWAT and eWAT remained unchanged after cold exposure (Figure S3D). However, histological analysis showed decreased browning of iWAT in *Mafb*$^{f/f}$::LysM-Cre mice compared to controls (Figure S3E); this could be attributed to MAFB regulation of apoptosis inhibitor of macrophages (AIM) in WAT, which could decrease lipolysis of WAT[16] and could further affect overall thermogenesis. Furthermore, IHC, histology, and RNA analysis using RT-qPCR of iBAT showed that *Mafb*$^{f/f}$::LysM-Cre mice UCP-1 protein levels were decreased (Figure 3B), iBAT having larger lipid droplets (Figure 3C) and reduced expression of functional BAT markers *Pparg*, *Cidea*, *Adrb3, Prdm16*, and *Lxrα* reported in earlier studies[4,22] (Figure 3D). RNA sequencing of the iBAT from the *Mafb*$^{f/f}$::LysM-Cre and *Mafb*$^{f/f}$ littermate mice exposed to cold for 10 days identified 109 downregulated and 191 upregulated genes, including *Mafb* and *Ucp1* (Figures 3E and 3F). Kyoto Encyclopedia of Genes and Genomes pathway analysis of the downregulated genes highlighted significant enrichment in thermogenesis and oxidative phosphorylation pathways (Figures S3F–S3G), confirming impaired thermogenic function in the BAT of *Mafb*$^{f/f}$::LysM-Cre mice and that in *Mafb*$^{f/f}$ mice.

Decreased SN density in BAT in *Mafb*$^{f/f}$::LysM-Cre mice

In the RNA sequencing data of mice continuously exposed to 10 days of cold, we observed some of the neurogenesis-related and neuronal signaling-related genes to be downregulated in *Mafb*$^{f/f}$::LysM-Cre mice compared with those in *Mafb*$^{f/f}$ mice (Figures S3H and S3I). To obtain further insights, we evaluated the density of SNs in BAT after 10 days of cold exposure using conventional IHC and 3-dimensional IHC (3DISCO) with an anti-tyrosine hydroxylase (TH) antibody (a widely used marker of sympathetic axons). We observed an ~35% decrease in SN axons in *Mafb*$^{f/f}$::LysM-Cre mice compared to *Mafb*$^{f/f}$ (Figure 4A). Interestingly, we found a marginal but significant decrease in SN density in *Mafb*$^{f/f}$::LysM-Cre mice housed under room temperature conditions (Figure 4B). 3DISCO imaging of iBAT of *Mafb*$^{f/f}$::LysM-Cre mice exposed to cold for 10 days also showed that the

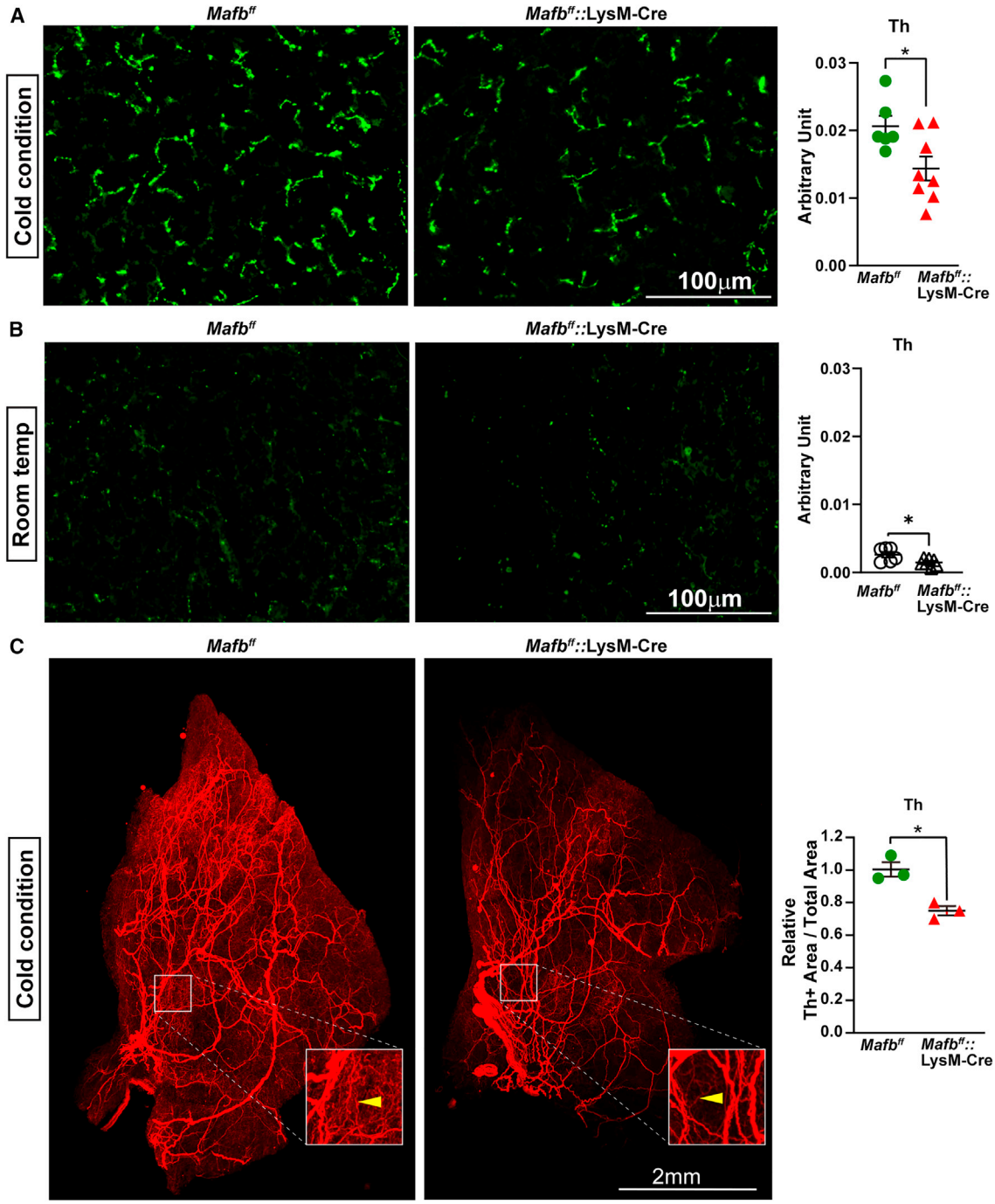

Figure 4. Reduced sympathetic nerve density in *Mafb*$^{f/f}$::LysM-Cre

Littermates of *Mafb*$^{f/f}$ and *Mafb*$^{f/f}$::LysM-Cre mice were exposed to cold for 10 days; iBAT was analyzed by IHC and 3DISCO staining.

(A) IHC with anti-Th antibody, quantifying Th$^+$ area/tissue area (*Mafb*$^{f/f}$, n = 6; *Mafb*$^{f/f}$::LysM-Cre, n = 8). Scale bar, 100 μm.

(B) IHC with anti-Th antibody, quantifying Th$^+$ area/tissue area (*Mafb*$^{f/f}$, n = 6; *Mafb*$^{f/f}$::LysM-Cre, n = 7). Scale bar, 100 μm.

(C) Three-dimensional (3D) full-focus images of iBAT, labeled with anti-Th antibody, imaged on Ultra Microscope-II, quantifying Th$^+$ area/tissue area relative to controls (n = 3 for each group). Scale bar, 2 mm.

Data are presented as mean ± SEM. *$p < 0.05$, Welch's t test.

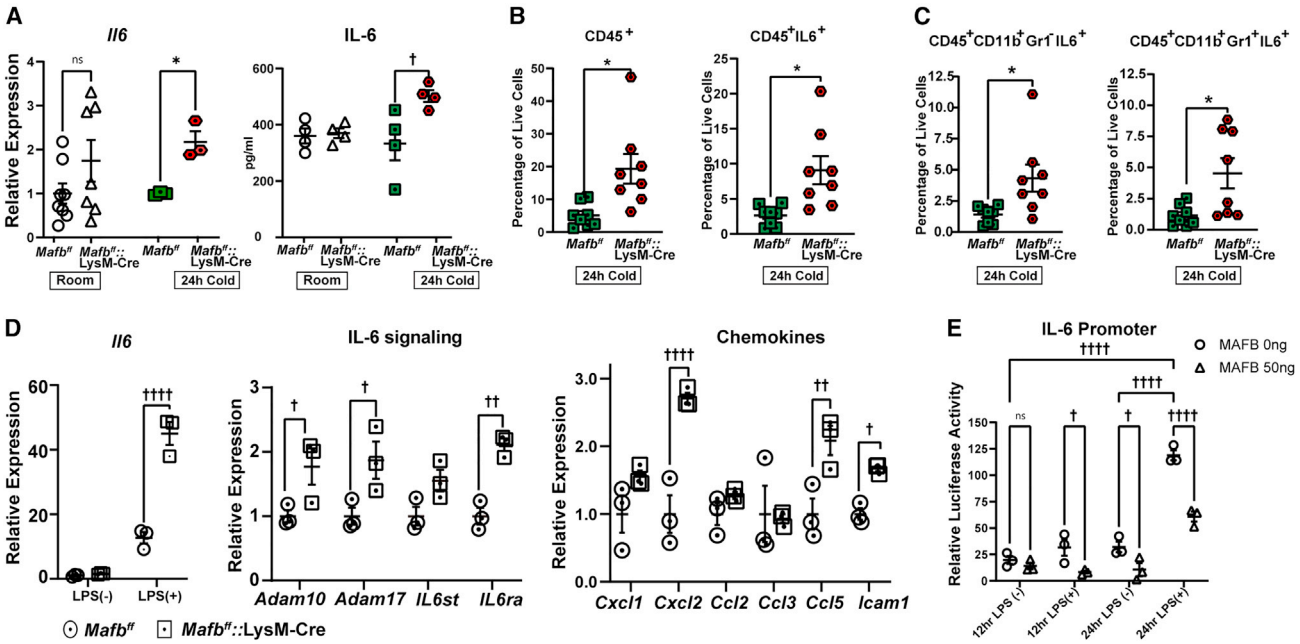

Figure 5. *Mafb* deficiency in macrophages has induced IL-6-mediated inflammation and accumulation of immune cells

Littermates of *Mafb*$^{f/f}$ and *Mafb*$^{f/f}$::LysM-Cre mice were exposed to 4°C cold for 10 days or 24 h 4°C or maintained at room temperature.

(A) iBAT, RT-qPCR of *Il6* for room temperature (n = 8,7 per group), and 24-h cold-exposure group (n = 3 per group); ELISA for the IL-6 protein of iBAT, room temperature, and 24-h cold-exposure group (n = 4 per group).

(B) Cytometry of iBAT-SVF fraction for 24-h cold exposure. Quantification of total CD45$^+$ cells and CD45$^+$IL-6$^+$ cells.

(C) Further gating of CD45$^+$IL-6$^+$ and quantifying IL-6$^+$ macrophages and granulocytes (n = 8 per group).

(D) *In vitro* culture of peritoneal macrophages from *Mafb*$^{f/f}$ and *Mafb*$^{f/f}$::LysM-Cre mice, and RT-qPCR for *Il6* with or without LPS, followed by RT-qPCR analysis for IL-6-signaling-related genes and chemokines responsible for the infiltration of monocytes and granulocytes without LPS (n = 3, per group).

(E) Luciferase reporter assay for IL-6 promoter activity in RAW 264.7 cells with or without LPS.

Data are presented as mean ± SEM. *$p < 0.05$, Welch's t test; $^{\dagger}p < 0.05$, $^{\dagger\dagger}p < 0.01$, $^{\dagger\dagger\dagger\dagger}p < 0.0001$; 2-way ANOVA with Holm-Sidak multiple comparison test; ns = not significant.

density of SN branching (marked by yellow arrow) was ~30% reduced compared with the *Mafb*$^{f/f}$ mice group (Figure 4C). Overall, these findings suggest that MAFB in macrophages has an impact on SN plasticity, particularly in regard to cold-induced axon branching, in BAT during cold acclimatization. In addition, we examined *Adrb2* RNA expression in our RNA sequencing data, which showed a trend toward upregulation (Figure S4D). This suggests that our hypothesis about MAFB regulation by sympathetic signaling may also hold true *in vivo*, particularly in conditions in which SN density decreases and *Mafb* deletion occurs in macrophages.

Suppression of IL-6 and inflammation in BAT by MAFB in macrophages

To explore the reduction in SN density in *Mafb*$^{f/f}$::LysM-Cre mice, we used the Enrichr tool to analyze RNA sequencing data for differentially upregulated genes in iBAT of *Mafb*$^{f/f}$::LysM-Cre mice and *Mafb*$^{f/f}$ mice after 10 days of cold exposure. The top three significant enriched terms in the mouse gene atlas database were related to inflammatory macrophages, and the enriched terms in Gene Ontology Molecular Pathway 2018 suggested neutrophil-mediated inflammation (Figures S4A and S4B). To further investigate this, we analyzed classical macrophage and adipose tissue inflammatory genes in iBAT using RT-qPCR. We observed a tendency for increase in *Il6*, *Il1β*, inflammatory genes, including *Arg1* and *Mac1* macrophages markers in *Mafb*$^{f/f}$::LysM-Cre mice compared to *Mafb*$^{f/f}$ mice (Figure S4C), indicating an inflammatory environment in BAT after 10 days of cold exposure.

Considering the slow pace of cold-induced increase in *Mafb*$^{f/f}$::LysM-Cre SN axon in mice during 10 days of cold exposure, which is accompanied by a mild inflammatory signature in BAT, we aimed to further assess BAT inflammation and investigate the adaptational and immunological changes at an early time point in BAT. For this purpose, we adopted a 24-h cold-exposure protocol, gradually decreasing the temperature during the first 4 h, followed by a constant 4°C. We found that *Il6* mRNA and protein were increased in *Mafb*$^{f/f}$::LysM-Cre mice after 24-h cold exposure compared to *Mafb*$^{f/f}$ mice; although there was no difference in IL-6 protein expression at room temperature, the *Il6* RNA showed a tendency toward an increase (Figure 5A). To identify IL-6-producing cells, we analyzed SVF from iBAT of 24-h cold-exposed mice, using flow cytometry between *Mafb*$^{f/f}$::LysM-Cre and *Mafb*$^{f/f}$ mice groups. The results revealed an overall increase in CD45$^+$ cells, and among CD45$^+$ cells, IL-6-expressing cells increased by 3.4-fold (Figures 5B and S5A–S5C). Further gating of CD45$^+$IL-6$^+$ cells revealed that IL-6-expressing cells were mainly macrophages or granulocytes (Figures 5C and

S5A–C). This suggests that *Mafb*-deficient macrophages in *Mafb*$^{f/f}$::LysM-Cre express a higher amount of IL-6, which further leads to the infiltration of IL-6-expressing granulocytes in the BAT. To further demonstrate the accumulation of macrophages using IHC, we first characterized the MAFB macrophage markers using an *Mafb*$^{+/gfp}$ mice BAT-SVF fraction using flow cytometry, which showed Mac2 as an appropriate marker for MAFB expressing macrophages (Figures S6A–S6D). The results showed that ~31% of macrophages express MAFB at room temperature, whereas at cold temperatures, >50% of macrophages express MAFB (Figure S6A–S6C). Similarly, IHC results of BAT sections from *Mafb*$^{f/f}$::LysM-Cre mice showed MAFB deficiency, resulting in an increased accumulation of macrophages (Figure S6E). To investigate the phenotype characteristic of these increased macrophages in *Mafb*-deficient mice, we looked at the RNA sequencing analysis of the upregulated genes, as described in Figure S4A, and identified the top enriched term as "macrophage peritoneal LPS (lipopolysaccharide) macrophage 1 h, 0 h, and 7 h" in cold-exposed mice BAT. Thus, we conducted *in vitro* peritoneal macrophage cultures and treated them with LPS. LPS treatment notably increased IL-6 expression in the peritoneal macrophages derived from *Mafb*$^{f/f}$::LysM-Cre mice (Figure 5D). Moreover, we detected upregulated gene expression related to IL-6 signaling in the peritoneal macrophages of *Mafb*$^{f/f}$::LysM-Cre. This upregulation included A disintegrin and metalloproteinase domain (ADAM)-containing proteins 10 and 17 (*Adam10*, *Adam17*), IL-6 receptor α (*Il6ra*), and IL-6 signal transducer (*Il6st*, also known as gp130) (Figure 5D). In addition, we observed elevated levels of chemokine C-X-C motif ligand 2, chemokine C-C motif ligand 5, and intercellular adhesion molecule 1, chemokines implicated in the recruitment and infiltration of monocytes and neutrophils (Figure 5D). ADAM10 and ADAM17 are known to cleave IL-6Rα from membrane-bound to soluble form. The soluble IL-6Rα can bind to inflammatory cells expressing only IL-6ST, enhancing IL-6 inflammatory signaling and macrophage accumulation in the tissue.[23] Interestingly, a previous study using luciferase reporter assay showed that MAFB directly binds to the IL-6 promoter, suppressing its expression in MIN6 cells.[24] Similarly, we investigated the effect of MAFB on the IL-6 promoter in a macrophage cell line (RAW 264.7), with or without LPS treatment, for 12 and 24 h. Our findings revealed that MAFB consistently reduces luciferase activity for the IL-6 promoter under all of the tested conditions (Figure 5E), suggesting that MAFB may regulate IL-6 in macrophages in both inflammatory and noninflammatory states. These results indicated that *Mafb* deficiency led to IL-6^{+} macrophage-mediated inflammation, granulocyte infiltration, and BAT dysfunction.

Reduced NGF-expression in *Mafb*$^{f/f}$::LysM-Cre mice, due to IL-6-mediated inflammation in BAT

A previous study demonstrated that IL-6 suppresses NGF expression in adipocytes differentiated from 3T3-L1 cell lines.[25] To evaluate the cause of the decrease in SN density in iBAT of our mouse model having IL-6-mediated proinflammatory conditions, we quantified the *Ngf* mRNA in the iBAT of the control *Mafb*$^{f/f}$::LysM-Cre mice, 24 h of cold-exposed, and 10 days of cold-exposed mice and compared them with similarly treated *Mafb*$^{f/f}$ mice (Figure 6A). The mRNA expression at room temperature was similar for the two groups (Figure 6A, left panel). In comparison, it was significantly decreased (Figure 6A, center panel) and showed a tendency to decrease (Figure 6A, right panel) in the *Mafb*$^{f/f}$::LysM-Cre mice iBAT after 24 h and 10 days of cold exposure, respectively. To identify the specific BAT cell type expressing *Ngf*, we analyzed *Ngf* mRNA levels in the SVF fraction of the 24-h cold-exposed mice. The mRNA level of *Ngf* was dramatically higher in the iBAT SVF fraction compared to that in the whole iBAT of *Mafb*$^{f/f}$ mice, and it was downregulated in the *Mafb*$^{f/f}$::LysM-Cre mice iBAT SVF fraction (Figure 6A, center panel). IHC of the BAT of 24-h cold-exposed mice revealed NGF-expressing cells organized in several clusters (indicated by the yellow arrow, Figure 6B, left panel of IHC image), potentially clusters of immature adipocytes, which were enriched in the SVF fraction. These cluster formations were smaller in size in *Mafb*$^{f/f}$::LysM-Cre mice iBAT compared with *Mafb*$^{f/f}$ mice, with increased macrophage populations (Figure 6B, right panel of IHC and quantification). Western blot analysis for NGF of iBAT of 24-h cold-exposed mice showed an NGF dimer band at 26 kDa, further confirming the RNA and IHC results (Figures 6C and S7A)

To explore NGF-expressing cell features, we analyzed single-cell RNA sequencing data from Gene expression omnibus Database: GSE207706.[21] The BAT-SVF fraction was sorted for adipocyte precursors by removing lineage-positive immune cells. We performed graph-based clustering, plotted the t-distributed stochastic neighbor embedding (t-SNE) plot for cell clusters, and classified them according to their gene expression markers (Figures 6D and S7B–S7E; Table S2). Notably, we identified *Ngf* expression in mainly two clusters of cells, *Trpv1*$^{+}$ vascular muscle smooth muscle cells (VSMCs) and *Pdgfrb*^{high} pericytes (Figure 6D, clusters 5 and 6, and Figures S7B–S7E), whereas some of the *Pdgfra*$^{+}$ adipose tissue stromal cells (ASCs) were also positive for *Ngf* expression (Figure 6D, cluster 1). Cold conditions increased NGF expression, especially in clusters 5 and 6 (Figure 6D). *Trpv1*$^{+}$ VSMCs are the progenitors of highly thermogenic brown adipocytes, in addition to *Pdgfra*$^{+}$ ASC progenitors,[26] whereas in the *Pdgfrb*^{high} pericytes, NGF production may be required for neurovascular coordination.[27] Although NGF expression in WAT eosinophils has been shown to respond to thermogenesis,[28] there is no NGF expression in lineage-positive immune cells in the BAT (Figure S7F). These results suggest that NGF expression reduction in *Mafb*$^{f/f}$::LysM-Cre could be linked to the abnormality of SN innervation.

Mafb$^{f/f}$::LysM-Cre mice phenotype associated with inefficient thermogenesis improved by treatment with anti-IL-6 receptor α antibodies

Our findings thus far suggested that increased IL-6 expression suppresses thermogenesis. To verify this, we administered an anti-IL-6 receptor α antibody (aIL-6Rα), which can block both *cis*- and *trans*-signaling of IL-6, and hypothesized that this treatment would rescue the *Mafb*$^{f/f}$::LysM-Cre phenotype. After 10 days of cold induction, the aIL-6Rα-treated group showed increased rectal temperature, decreased body weight change, increased relative VO_2, and enhanced energy metabolism (Figures 7A–7D). *UCP-1* expression in iBAT was higher in the aIL-6Rα-treated group (Figures 7E and 7F). These results suggest

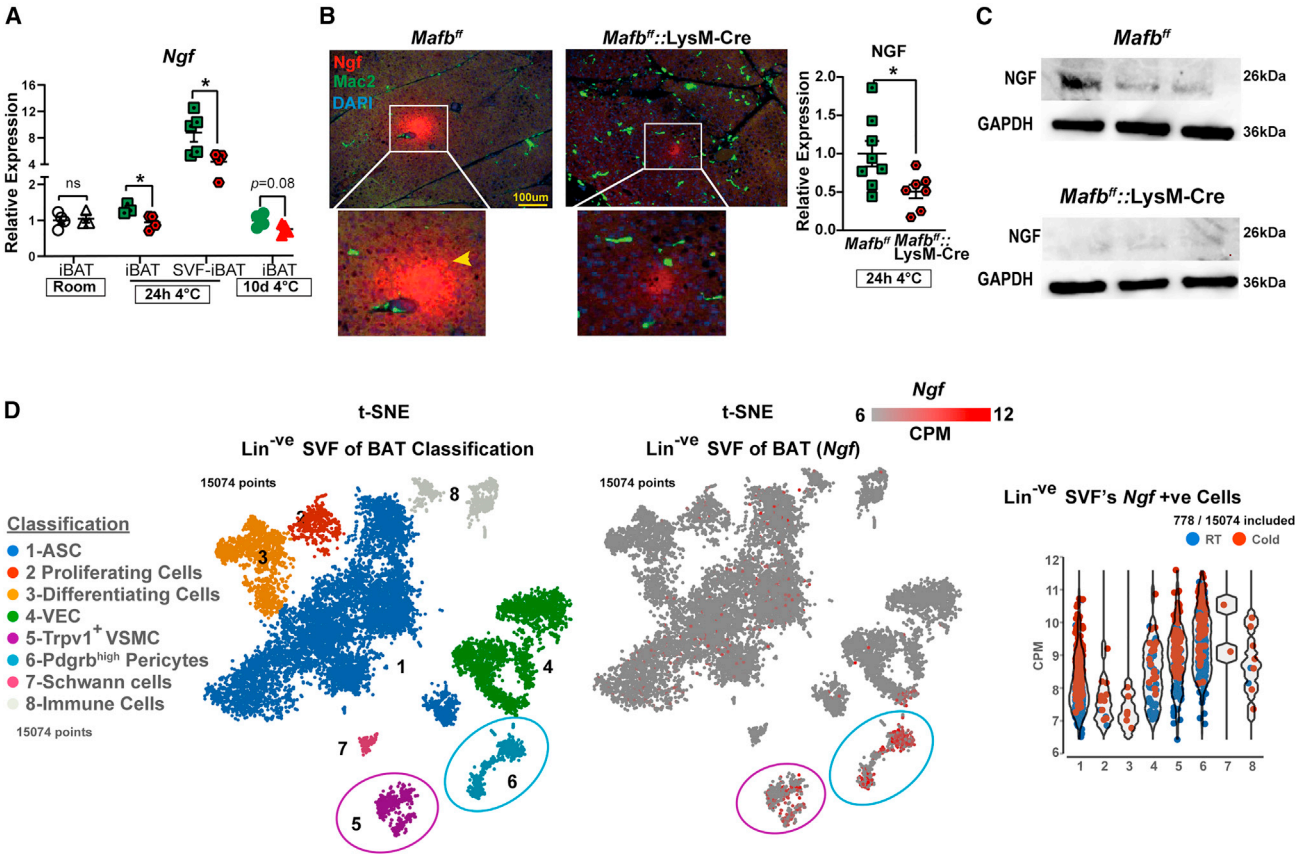

Figure 6. IL-6-mediated inflammation in BAT reduced the NGF expression in *Mafb*$^{f/f}$::LysM-Cre mice, which is important for cold-induced SN plasticity

Littermates of *Mafb*$^{f/f}$ and *Mafb*$^{f/f}$::LysM-Cre mice were exposed to cold for 10 days or 24 h, or maintained at room temperature. Single-cell RNA sequencing data were analyzed for lineage-negative room temperature and 4-day cold-exposed mice.

(A) iBAT, RT-qPCR for *Ngf* in various conditions and iBAT-SVF (n = 3–5 per group).

(B) IHC of NGF and quantification of iBAT, of 24-h cold-exposed mice (n = 8 per group). Scale bar, 100 μm.

(C) Western blot NGF of iBAT of 24-h cold-exposed mice (n = 3).

(D) t-SNE plot for lineage-negative cells, *Ngf* expression, and violin plot of *Ngf*$^{+}$ cells for each cell type.

Data are presented as mean ± SEM. Welch's t test, *p < 0.05.

that aIL-6Rα antibody treatment could rescue the effect of *Mafb* deficiency in macrophages by blocking IL-6 signaling leading to the upregulation of Ucp1 expression and increasing body temperature in *Mafb*$^{f/f}$::LysM-Cre mice.

Furthermore, 3DISCO and conventional IHC using the anti-TH antibody in iBAT showed an increase in SN density by >1.5-fold (Figures 7G and 7H). IHC results showed increased NGF^{+} cell clusters and decreased macrophages in aIL-6Ra-treated iBAT (Figure 7I). RT-qPCR results showed that *Ngf* RNA levels moderately increased (Figure 7J). These results suggest that aIL-6Ra antibodies restore sympathetic axon density by blocking IL-6 inflammatory effects from *Mafb*-deficient macrophages in *Mafb*$^{f/f}$::LysM-Cre mice iBAT.

DISCUSSION

Our findings suggest that MAFB increases NGF expression by suppressing IL-6 expression in macrophages following cold stimulation, subsequently promoting SN density and inducing thermogenesis. NGF belongs to the family of neurotrophic factors that includes Neurotrophin-3 (NT-3), brain-derived neurotrophic factor, and NT-4/5. It is expressed in the CNS and non-neuronal cells of the peripheral nervous system to promote the survival and growth of neuronal axons. NGF and NT-3 have been reported to regulate SN density in BAT.[9,27,29–31] NGF expression is induced after cold exposure in both BAT and WAT.[9,31,32] NT-3 does not increase in BAT after cold exposure and remains unchanged in iWAT, whereas NGF levels increased, and neutralizing the NGF resulted in the loss of cold-induced increase in SN in the iWAT.[29,32] This suggests that NGF is required for cold-induced SN plasticity, whereas both NGF and NT-3 are also required for the developmental plasticity of SN innervation. In our study, we observed an increase in NGF expression in BAT after 24 h of cold exposure, with a significant difference between control and *Mafb*$^{f/f}$::LysM-Cre mice.[29,33] These findings suggest that the decreased

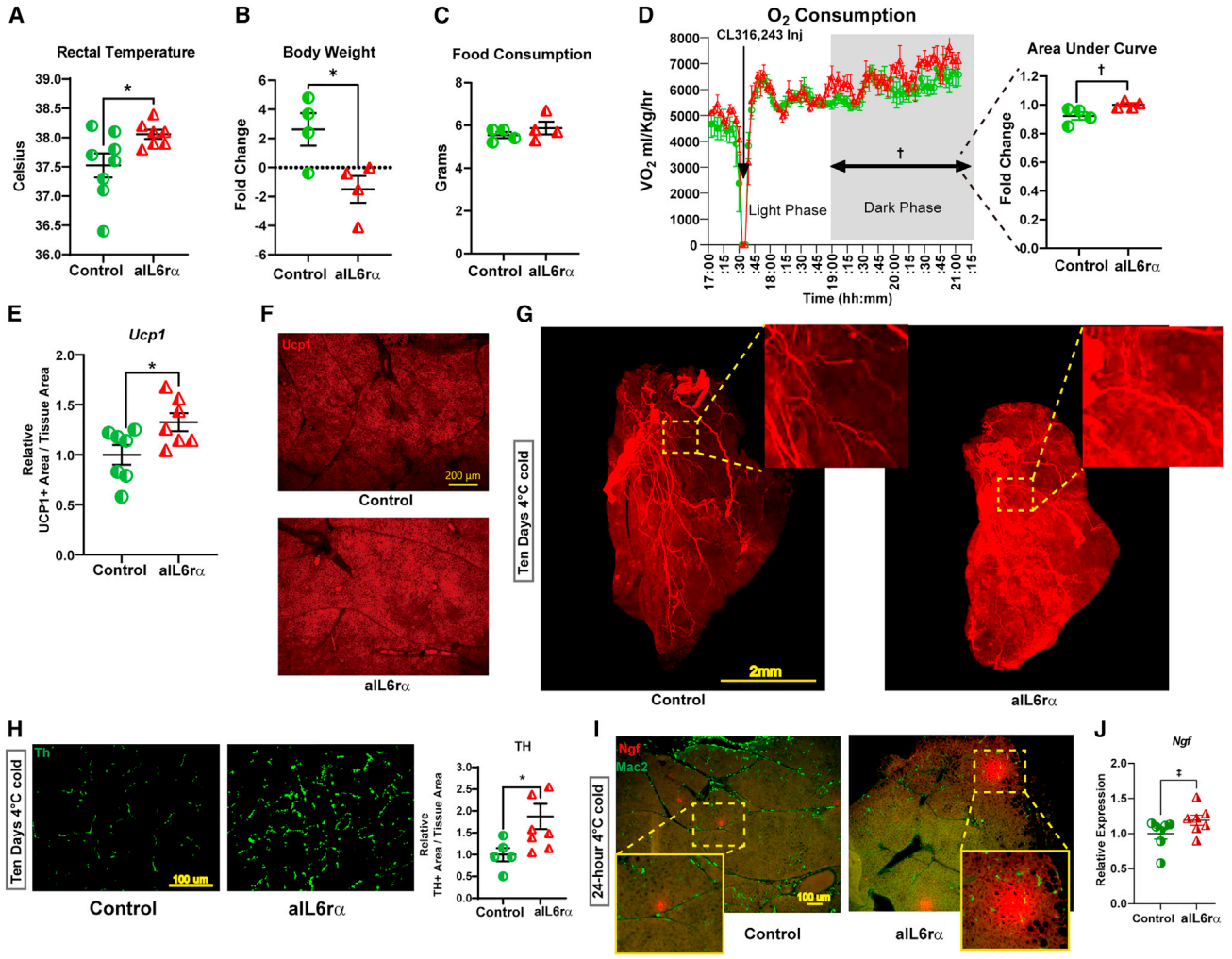

Figure 7. *Mafb*$^{f/f}$::LysM-Cre mice thermogenesis is improved with increase in SN density by aIL-6Rα treatment

Mafb$^{f/f}$::LysM-mice were divided into aIL-6Rα treatment and rat immunoglobulin G1 (IgG1) isotype/PBS as control groups and exposed to 4°C for 10 days.

(A) Rectal temperature on day 10 (n = 8,7 per group respectively, control = rat IgG1).

(B) Percentage body weight change on day 10 (n = 4 per group, control = PBS).

(C) Average daily food consumption during the 10 days of cold exposure (n = 4 per group, control = PBS).

(D) Relative VO_2 on day 10 after β3 agonist injection (1 mg/kg of body weight) and area under the curve quantification for dark phase (n = 4 per group, control = PBS).

(E) iBAT Ucp1 gene expression after cold exposure (n = 7 per group, control = rat IgG1).

(F) iBAT analyzed by IHC for Ucp1 expression (control = rat IgG1).

(G) 3D full-focus images of iBAT, immunolabeled by anti-Th antibody (n = 3 for each group, control = rat IgG1). Scale bar, 2 mm.

(H) IHC with anti-Th antibody and Th$^+$ area quantification (n = 5,7 per group respectively, control = rat IgG1). Scale bar, 100 μm.

(I) IHC using an anti-NGF antibody (control = rat IgG1). Scale bar, 100 μm.

(J) RT-qPCR results for Ngf (control = rat IgG1).

Data are presented as mean ± SEM. *p < 0.05 Welch's t test, †p < 0.05 Mann-Whitney test, ‡p < 0.05 Welch's t test 1-tailed.

SN density in *Mafb*$^{f/f}$::LysM-Cre mice can be attributed to a decrease in NGF levels.

The NGF-producing cell types in BAT were unknown; IHC of BAT showed that NGF$^+$ cells were organized in several clusters throughout the tissue. Moreover, the enrichment of NGF expression in SVF, from which large cells were removed, suggested that the expressing cells may be derived from relatively small undifferentiated adipocytes. Single-cell RNA sequencing analysis of SVF of BAT[26] showed that the NGF-expressing cells were *Trpv1*$^+$ VSMCs, *Pdgfrb*^{high} pericytes, and some of the *Pdgfra*$^+$ ASCs. A recent report indicated that *Trpv1*$^+$ VSMCs were the progenitors of highly thermogenic brown adipocytes other than the *Pdgfra*$^+$ ASCs.[34] NGF expression by these cell populations may be the reason for increased neurite growth during cold exposure. Furthermore, NGF expression by pericytes could be required for neurovascular coordination.

A recent study reported NGF-TrkA signaling in BAT/WAT for neurovascular coordination.[27] However, we could only detect clustered cells positive for NGF, a characteristic of *Trpv1*$^{+}$ VSMC or *Pdgfra*$^{+}$ ASC populations. The pericytes possibly secrete NGF immediately after expression, and their scattered distribution throughout BAT makes it challenging to be detected by IHC, whereas NGF expression by clustered cells could be detected.

IL-6 has diverse functions, and its effects depend on the cells expressing it and the presence of membrane-bound or soluble IL-6Rα. However, the role of IL-6-expressing cell types in BAT remains unclear. Global Il6-KO mice showed lower oxygen consumption and body temperature at low temperatures.[35] In addition, Il6-KO in the lateral parabrachial nucleus led to decreased heat production in BAT and increased body weight.[36] Thus, IL-6 secretion in the CNS enhances adipose tissue metabolism. In BAT, both adipocytes and macrophages express IL-6. Under sympathetic stimuli, BAT adipocytes produce IL-6 in response to stress, aiding insulin sensitivity and gluconeogenesis for the fight-or-flight response.[37–40] In pathological conditions such as obesity, IL-6 contributes to inflammation, whereas under normal circumstances, it promotes insulin sensitivity and lipolysis.[41–43] Recent studies revealed that ADAM10/17 play an essential role in immune cell accumulation by increasing soluble IL-6ST and promoting IL-6 *trans*-signaling.[23,37] IL-6 signaling can further recruit neutrophils in inflammatory conditions.[44] Our study indicates that *Mafb* deficiency increases IL-6 production and signaling molecules, including IL-6Rα and ADAM10/17. Increased IL6-Rα and ADAM10/17 contributed to inflammation by promoting IL-6 *trans*-signaling and the recruitment of neutrophils and macrophages in BAT through the induction of chemokines that facilitate neutrophil and monocyte trafficking. A recent study by Amin et al. showed that the loss of ADAM17 in adipocytes attenuates thermogenesis through the cleavage of semaphorin 4B, thereby suppressing thermogenesis-related genes directly in adipocytes.[45] Our previous finding that *Mafb*$^{f/f}$::LysM-Cre mice resulted in increased body weight in HFD-fed mice with an increase in macrophages further suggests that *Mafb* deficiency in macrophages results in the accumulation of inflammatory M1-like macrophages in adipose tissue.[16] Furthermore, in the present study, we found that the decrease in sympathetic tone observed in *Mafb*$^{f/f}$::LysM-Cre mice was restored by treatment with anti-IL-6Rα antibodies, indicating that IL-6 is involved in the regulation of cold-induced SN density of BAT by decreasing NGF. Notably, a study published in 2004 reported that NGF expression was suppressed when IL-6 was added to 3T3-L1 mouse progenitor adipocytes *in vitro*.[25] We hypothesize that IL-6 signaling may act on *Trpv1*$^{+}$ VSMCs, *Pdgfra*$^{+}$ ASCs, or *Pdgrb*^{high} pericytes to suppress NGF expression directly or indirectly by creating an inflammatory environment in the BAT.

We demonstrated that *Mafb* deficiency in macrophages resulted in a substantial upregulation of IL-6 expression. Intriguingly, a previous study reported that MAFB has a binding site within the IL-6 promoter region and, upon direct binding to this region in insulinoma MIN6 cells, suppresses IL-6 expression.[46] Similarly, our IL-6 promoter analysis using the luciferase assay suggests that MAFB in RAW 264.7 macrophages also represses the IL-6 expression. In addition, MAFB can repress the function of interferon regulatory factor 3 (IRF3); however, because IRF3 regulates IL-6,[47] IL-6 production may be increased by the activation of IRF3 in *Mafb*$^{f/f}$::LysM-Cre mice. In addition, we demonstrated that cold stimulation nearly doubled *Mafb* expression in BAT. Our *in vitro* experiments showed that *Mafb* expression in macrophages increased in response to noradrenaline stimulation, potentially via adrenergic β2 receptor activation. The expression of adrenergic β2 receptors in macrophages increased because noradrenaline receptors regulate the polarization of immunostimulatory M1 macrophages into immunosuppressive M2 macrophages.[48] This observation is consistent with previous studies showing that MAFB is highly expressed in M2 macrophages.[49] Interestingly, when we treated *Mafb*-deficient macrophages with noradrenaline, the noradrenaline signaling failed to increase MAFB expression in these macrophages, resulting in the dysregulation of β2 receptor expression. Furthermore, IL-6 expression is suppressed in macrophages that receive noradrenaline β2 receptor signals.[50] Therefore, macrophages receive noradrenergic stimulation via β2 receptors to induce *Mafb* expression, suppress IL-6 expression, and increase NGF expression, thus leading to sympathetic development. Because NGF increases IL-6 expression in bone marrow stromal cells,[51] MAFB could probably suppress IL-6 expression under severe conditions, such as cold stimulation, thereby activating NGF and promoting sympathetic nerve development.

MAFB in macrophages is proposed as being crucial for homeostatic functions related to inflammation suppression, apoptotic cell removal, and metabolic syndrome,[14] indicating that MAFB is recruited as response molecules to bodily abnormalities, and its expression can be upregulated by various nuclear receptor transcription factor agonists.[14] MAFB-mediated homeostatic and adaptive mechanisms in macrophages may enable the development of therapeutic tools to treat obesity and metabolic diseases. By targeting MAFB, we could address metabolic diseases through multiple mechanisms—in thermoneutral environments by inhibiting lipogenesis in WAT via AIM[16] and in cold environments by enhancing SN density and regulating anti-inflammatory homeostasis via IL-6 suppression in BAT, as demonstrated in this study.

Limitations of the study

Although our study has provided significant insights into the regulatory role of MAFB in macrophage-mediated BAT thermogenesis, it is important to note certain limitations. To mitigate estrous cycle-related hormonal variations, we exclusively used male mice for our macrophage-specific and adipose tissue-specific *Mafb*-deficient models. This choice was aimed at reducing result variability during cold exposure, although similar Ucp1 decreases were observed in the BAT of inducible whole-body *Mafb*-deficient mice even at room temperature, suggesting similar results may be observed in both sexes. In addition, although our focus was primarily on BAT thermogenesis, we acknowledge the potential contributions of subcutaneous WAT in thermogenesis, which were not extensively explored in our research.

STAR★METHODS

Detailed methods are provided in the online version of this paper and include the following:

- KEY RESOURCES TABLE
- RESOURCE AVAILABILITY
  - Lead contact
  - Materials availability
  - Data and code availability
- EXPERIMENTAL MODEL AND STUDY PARTICIPANT DETAILS
  - Animals
- METHOD DETAILS
  - Cold exposure experiments
  - RT-qPCR
  - Measurement of rectal and skin temperature
  - Intracapsular BAT temperature recording
  - Relative VO_2 measurement
  - RNA sequencing
  - Single cell RNA sequencing analysis
  - Immunohistochemistry (IHC)
  - 3DISCO staining and imaging
  - Hematoxylin and eosin (HE) staining
  - IL-6 cytokine ELISA
  - Western blot
  - Isolation of BAT SVF
  - Flow cytometry and intracellular IL-6 staining
  - Luciferase reporter assays
  - Anti-IL-6Rα rescue experiments
- QUANTIFICATION AND STATISTICAL ANALYSIS

SUPPLEMENTAL INFORMATION

Supplemental information can be found online at https://doi.org/10.1016/j.celrep.2024.113978.

ACKNOWLEDGMENTS

This work was supported by the Ministry of Education and Sports of Japan (MEXT); the Ministry of Education, Culture, Sports, Science and Technology of Japan under grant nos. 26221004, 25860205, 23118504, 16K18398, 19K07499, 19H00966, 23K05586, and 19K07499; the Uehara Memorial Foundation; the Takeda Science Foundation; the Takamatsunomiya Cancer Foundation under grant no. 15–24724(M.H.); and the World Premier International Research Center Initiative (WPI), MEXT, Japan. We acknowledge the School of Integrative & Global Majors (SIGMA)'s Ph.D. in Human Biology Program, University of Tsukuba, for the student support. We thank Naomi Nagashima and Shohei Nakayama from Miltenyi Biotech (Tokyo, Japan) for 3DISCO imaging assistance using the Ultra Microscope-II and Chugai Pharmaceutical (Tokyo, Japan) for providing the aIL-6Rα antibodies. We acknowledge Masami Ojima for her technical support, and Yuri Inoue for supporting the *Mafb*$^{f/f}$::LysM-Cre mice colony management.

AUTHOR CONTRIBUTIONS

S.T., M.H., and M.K.Y. conceptualized the study; M.K.Y., M.I., and M.H. designed the study; M.K.Y., M.I., N.G., F.N.S., T.H., Z.J.S., O.S., O.O., and W.L. performed the experiments; M.K.Y., M.I., A.K., and C.-W.L. analyzed the data; M.K.Y., M.I., K.K., and M.H. interpreted the data; M.K.Y., M.I., and E.C.M. wrote the initial manuscript; S.T. and M.H. wrote the final manuscript; S.T. and M.H. supervised the study.

DECLARATION OF INTERESTS

The authors declare no competing interests.

Received: May 10, 2023
Revised: January 28, 2024
Accepted: March 5, 2024
Published: March 22, 2024

REFERENCES

1. Bartness, T.J., Vaughan, C.H., and Song, C.K. (2010). Sympathetic and sensory innervation of brown adipose tissue. Int. J. Obes. *34*, S36–S42, Suppl 1. https://doi.org/10.1038/ijo.2010.182.
2. Murano, I., Barbatelli, G., Giordano, A., and Cinti, S. (2009). Noradrenergic parenchymal nerve fiber branching after cold acclimatisation correlates with brown adipocyte density in mouse adipose organ. J. Anat. *214*, 171–178. https://doi.org/10.1111/j.1469-7580.2008.01001.x.
3. Klingenberg, M., Echtay, K.S., Bienengraeber, M., Winkler, E., and Huang, S.G. (1999). Structure–Function Relationship in UCP1. Int. J. Obes. Relat. Metab. Disord. *23*, S24–S29. https://doi.org/10.1038/sj.ijo.0800939.
4. Wolf, Y., Boura-Halfon, S., Cortese, N., Haimon, Z., Sar Shalom, H., Kuperman, Y., Kalchenko, V., Brandis, A., David, E., Segal-Hayoun, Y., et al. (2017). Brown-adipose-tissue macrophages control tissue innervation and homeostatic energy expenditure. Nat. Immunol. *18*, 665–674. https://doi.org/10.1038/ni.3746.
5. Cereijo, R., Gavaldà-Navarro, A., Cairó, M., Quesada-López, T., Villarroya, J., Morón-Ros, S., Sánchez-Infantes, D., Peyrou, M., Iglesias, R., Mampel, T., et al. (2018). CXCL14, a Brown adipokine that mediates brown-fat-to-macrophage communication in thermogenic adaptation. Cell Metab. *28*, 750–763.e6. https://doi.org/10.1016/j.cmet.2018.07.015.
6. Nguyen, K.D., Qiu, Y., Cui, X., Goh, Y.P.S., Mwangi, J., David, T., Mukundan, L., Brombacher, F., Locksley, R.M., and Chawla, A. (2011). Alternatively activated macrophages produce catecholamines to sustain adaptive thermogenesis. Nature *480*, 104–108. https://doi.org/10.1038/nature10653.
7. Ruiz De Azua, I., Mancini, G., Srivastava, R.K., Rey, A.A., Cardinal, P., Tedesco, L., Zingaretti, C.M., Sassmann, A., Quarta, C., Schwitter, C., et al. (2017). Adipocyte cannabinoid receptor CB1 regulates energy homeostasis and alternatively activated macrophages. J. Clin. Invest. *127*, 4148–4162. https://doi.org/10.1172/jci83626.
8. Pirzgalska, R.M., Seixas, E., Seidman, J.S., Link, V.M., Sánchez, N.M., Mahú, I., Mendes, R., Gres, V., Kubasova, N., Morris, I., et al. (2017). Sympathetic neuron-associated macrophages contribute to obesity by importing and metabolizing norepinephrine. Nat. Med. *23*, 1309–1318. https://doi.org/10.1038/nm.4422.
9. Nisoli, E., Tonello, C., Benarese, M., Liberini, P., and Carruba, M.O. (1996). Expression of nerve growth factor in brown adipose tissue: implications for thermogenesis and obesity. Endocrinology *137*, 495–503. https://doi.org/10.1210/endo.137.2.8593794.
10. Zeng, X., Ye, M., Resch, J.M., Jedrychowski, M.P., Hu, B., Lowell, B.B., Ginty, D.D., and Spiegelman, B.M. (2019). Innervation of thermogenic adipose tissue via a calsyntenin 3β–S100b axis. Nature *569*, 229–235. https://doi.org/10.1038/s41586-019-1156-9.
11. Yoon, Y.-S., Tsai, W.-W., Van De Velde, S., Chen, Z., Lee, K.-F., Morgan, D.A., Rahmouni, K., Matsumura, S., Wiater, E., Song, Y., and Montminy, M. (2018). cAMP-inducible coactivator CRTC3 attenuates brown adipose tissue thermogenesis. Proc. Natl. Acad. Sci. USA *115*, E5289–E5297. https://doi.org/10.1073/pnas.1805257115.
12. Kataoka, K., Fujiwara, K.T., Noda, M., and Nishizawa, M. (1994). MafB, a new Maf family transcription activator that can associate with Maf and Fos but not with Jun. Mol. Cell Biol. *14*, 7581–7591. https://doi.org/10.1128/mcb.14.11.7581-7591.1994.

13. Moriguchi, T., Hamada, M., Morito, N., Terunuma, T., Hasegawa, K., Zhang, C., Yokomizo, T., Esaki, R., Kuroda, E., Yoh, K., et al. (2006). MafB is essential for renal development and F4/80 expression in macrophages. Mol. Cell Biol. *26*, 5715–5727. https://doi.org/10.1128/MCB.00001-06.

14. Hamada, M., Tsunakawa, Y., Jeon, H., Yadav, M.K., and Takahashi, S. (2020). Role of MafB in macrophages. Exp. Anim. *69*, 1–10. https://doi.org/10.1538/expanim.19-0076.

15. Tran, M.T.N., Hamada, M., Jeon, H., Shiraishi, R., Asano, K., Hattori, M., Nakamura, M., Imamura, Y., Tsunakawa, Y., Fujii, R., et al. (2017). MafB is a critical regulator of complement component C1q. Nat. Commun. *8*, 1700. https://doi.org/10.1038/s41467-017-01711-0.

16. Tran, M.T.N., Hamada, M., Nakamura, M., Jeon, H., Kamei, R., Tsunakawa, Y., Kulathunga, K., Lin, Y.Y., Fujisawa, K., Kudo, T., and Takahashi, S. (2016). MafB deficiency accelerates the development of obesity in mice. FEBS Open Bio *6*, 540–547. https://doi.org/10.1002/2211-5463.12058.

17. Hamada, M., Nakamura, M., Tran, M.T.N., Moriguchi, T., Hong, C., Ohsumi, T., Dinh, T.T.H., Kusakabe, M., Hattori, M., Katsumata, T., et al. (2014). MafB promotes atherosclerosis by inhibiting foam-cell apoptosis. Nat. Commun. *5*, 3147. https://doi.org/10.1038/ncomms4147.

18. Cinti, S., Mitchell, G., Barbatelli, G., Murano, I., Ceresi, E., Faloia, E., Wang, S., Fortier, M., Greenberg, A.S., and Obin, M.S. (2005). Adipocyte death defines macrophage localization and function in adipose tissue of obese mice and humans. J. Lipid Res. *46*, 2347–2355. https://doi.org/10.1194/jlr.M500294-JLR200.

19. Cinti, S. (2011). Between brown and white: Novel aspects of adipocyte differentiation. Ann. Med. *43*, 104–115. https://doi.org/10.3109/07853890.2010.535557.

20. Fujisaka, S. (2021). The role of adipose tissue M1/M2 macrophages in type 2 diabetes mellitus. Diabetol. Int. *12*, 74–79. https://doi.org/10.1007/s13340-020-00482-2.

21. Burl, R.B., Rondini, E.A., Wei, H., Pique-Regi, R., and Granneman, J.G.. Deconstructing Cold-Induced Brown Adipocyte Neogenesis in Mice. 2022. Gene Expression Omnibus, NCBI Database, GSE207706. https://www.ncbi.nlm.nih.gov/geo/query/acc.cgi?acc=GSE207706.

22. Harms, M.J., Ishibashi, J., Wang, W., Lim, H.-W., Goyama, S., Sato, T., Kurokawa, M., Won, K.-J., and Seale, P. (2014). Prdm16 Is required for the maintenance of brown adipocyte identity and function in adult mice. Cell Metab. *19*, 593–604. https://doi.org/10.1016/j.cmet.2014.03.007.

23. Kraakman, M.J., Kammoun, H.L., Allen, T.L., Deswaerte, V., Henstridge, D.C., Estevez, E., Matthews, V.B., Neill, B., White, D.A., Murphy, A.J., et al. (2015). Blocking IL-6 trans-Signaling Prevents High-Fat Diet-Induced Adipose Tissue Macrophage Recruitment but Does Not Improve Insulin Resistance. Cell Metab. *21*, 403–416. https://doi.org/10.1016/j.cmet.2015.02.006.

24. Zhu, M., Wei, Y., Geißler, C., Abschlag, K., Corbalán Campos, J., Hristov, M., Möllmann, J., Lehrke, M., Karshovska, E., and Schober, A. (2017). Hyperlipidemia-Induced MicroRNA-155-5p Improves beta-Cell Function by Targeting Mafb. Diabetes *66*, 3072–3084. https://doi.org/10.2337/db17-0313.

25. Peeraully, M.R., Jenkins, J.R., and Trayhurn, P. (2004). NGF gene expression and secretion in white adipose tissue: regulation in 3T3-L1 adipocytes by hormones and inflammatory cytokines. Am. J. Physiol. Endocrinol. Metab. *287*, E331–E339. https://doi.org/10.1152/ajpendo.00076.2004.

26. Burl, R.B., Rondini, E.A., Wei, H., Pique-Regi, R., and Granneman, J.G. (2022). Deconstructing cold-induced brown adipocyte neogenesis in mice. Elife *11*, e80167. https://doi.org/10.7554/elife.80167.

27. Daquinag, A.C., Gao, Z., Yu, Y., and Kolonin, M.G. (2022). Endothelial TrkA coordinates vascularization and innervation in thermogenic adipose tissue and can be targeted to control metabolism. Mol. Metab. *63*, 101544. https://doi.org/10.1016/j.molmet.2022.101544.

28. Meng, X., Qian, X., Ding, X., Wang, W., Yin, X., Zhuang, G., and Zeng, W. (2022). Eosinophils regulate intra-adipose axonal plasticity. Proc. Natl. Acad. Sci. USA *119*, e2112281119. https://doi.org/10.1073/pnas.2112281119.

29. Cui, X., Jing, J., Wu, R., Cao, Q., Li, F., Li, K., Wang, S., Yu, L., Schwartz, G., Shi, H., et al. (2021). Adipose tissue-derived neurotrophic factor 3 regulates sympathetic innervation and thermogenesis in adipose tissue. Nat. Commun. *12*, 5362. https://doi.org/10.1038/s41467-021-25766-2.

30. Néchad, M., Ruka, E., and Thibault, J. (1994). Production of nerve growth factor by brown fat in culture: relation with the in vivo developmental stage of the tissue. Comp. Biochem. Physiol. A Comp. Physiol. *107*, 381–388. https://doi.org/10.1016/0300-9629(94)90396-4.

31. Camerino, C., Conte, E., Caloiero, R., Fonzino, A., Carratù, M., Lograno, M.D., and Tricarico, D. (2017). Evaluation of short and long term cold stress challenge of nerve grow factor, brain-derived neurotrophic factor, osteocalcin and oxytocin mRNA expression in BAT, brain, bone and reproductive tissue of male mice using real-time PCR and linear correlation analysis. Front. Physiol. *8*, 1101. https://doi.org/10.3389/fphys.2017.01101.

32. Cao, Y., Wang, H., and Zeng, W. (2018). Whole-tissue 3D imaging reveals intra-adipose sympathetic plasticity regulated by NGF-TrkA signal in cold-induced beiging. Protein Cell *9*, 527–539. https://doi.org/10.1007/s13238-018-0528-5.

33. Crowley, C., Spencer, S.D., Nishimura, M.C., Chen, K.S., Pitts-Meek, S., Armanini, M.P., Ling, L.H., McMahon, S.B., Shelton, D.L., Levinson, A.D., and Phillips, H.S. (1994). Mice lacking nerve growth factor display perinatal loss of sensory and sympathetic neurons yet develop basal forebrain cholinergic neurons. Cell *76*, 1001–1011. https://doi.org/10.1016/0092-8674(94)90378-6.

34. Shamsi, F., Piper, M., Ho, L.-L., Huang, T.L., Gupta, A., Streets, A., Lynes, M.D., and Tseng, Y.-H. (2021). Vascular smooth muscle-derived Trpv1+ progenitors are a source of cold-induced thermogenic adipocytes. Nat. Metab. *3*, 485–495. https://doi.org/10.1038/s42255-021-00373-z.

35. Wernstedt, I., Edgley, A., Berndtsson, A., Fäldt, J., Bergström, G., Wallenius, V., and Jansson, J.O. (2006). Reduced stress- and cold-induced increase in energy expenditure in interleukin-6-deficient mice. Am. J. Physiol. Regul. Integr. Comp. Physiol. *291*, R551–R557. https://doi.org/10.1152/ajpregu.00514.2005.

36. Mishra, D., Richard, J.E., Maric, I., Porteiro, B., Häring, M., Kooijman, S., Musovic, S., Eerola, K., López-Ferreras, L., Peris, E., et al. (2019). Parabrachial Interleukin-6 Reduces Body Weight and Food Intake and Increases Thermogenesis to Regulate Energy Metabolism. Cell Rep. *26*, 3011–3026.e5. https://doi.org/10.1016/j.celrep.2019.02.044.

37. Han, M.S., White, A., Perry, R.J., Camporez, J.-P., Hidalgo, J., Shulman, G.I., and Davis, R.J. (2020). Regulation of adipose tissue inflammation by interleukin 6. Proc. Natl. Acad. Sci. USA *117*, 2751–2760. https://doi.org/10.1073/pnas.1920004117.

38. Burýsek, L., and Houštěk, J. (1997). β-Adrenergic stimulation of interleukin-1α and interleukin-6 expression in mouse brown adipocytes. FEBS Lett. *411*, 83–86. https://doi.org/10.1016/s0014-5793(97)00671-6.

39. Qing, H., Desrouleaux, R., Israni-Winger, K., Mineur, Y.S., Fogelman, N., Zhang, C., Rashed, S., Palm, N.W., Sinha, R., Picciotto, M.R., et al. (2020). Origin and Function of Stress-Induced IL-6 in Murine Models. Cell *182*, 372–387.e14. https://doi.org/10.1016/j.cell.2020.05.054.

40. Mauer, J., Chaurasia, B., Goldau, J., Vogt, M.C., Ruud, J., Nguyen, K.D., Theurich, S., Hausen, A.C., Schmitz, J., Brönneke, H.S., et al. (2014). Signaling by IL-6 promotes alternative activation of macrophages to limit endotoxemia and obesity-associated resistance to insulin. Nat. Immunol. *15*, 423–430. https://doi.org/10.1038/ni.2865.

41. Sindhu, S., Thomas, R., Shihab, P., Sriraman, D., Behbehani, K., and Ahmad, R. (2015). Obesity Is a Positive Modulator of IL-6R and IL-6 Expression in the Subcutaneous Adipose Tissue: Significance for Metabolic Inflammation. PLoS One *10*, e0133494. https://doi.org/10.1371/journal.pone.0133494.

42. Trujillo, M.E., and Scherer, P.E. (2006). Adipose tissue-derived factors: impact on health and disease. Endocr. Rev. *27*, 762–778. https://doi.org/10.1210/er.2006-0033.

43. Weisberg, S.P., McCann, D., Desai, M., Rosenbaum, M., Leibel, R.L., and Ferrante, A.W., Jr. (2003). Obesity is associated with macrophage accumulation in adipose tissue. J. Clin. Invest. *112*, 1796–1808. https://doi.org/10.1172/JCI19246.

44. Fielding, C.A., Mcloughlin, R.M., Mcleod, L., Colmont, C.S., Najdovska, M., Grail, D., Ernst, M., Jones, S.A., Topley, N., and Jenkins, B.J. (2008). IL-6 regulates neutrophil trafficking during acute inflammation via STAT3. J. Immunol. *181*, 2189–2195. https://doi.org/10.4049/jimmunol.181.3.2189.

45. Amin, A., Badenes, M., Tüshaus, J., de Carvalho, É., Burbridge, E., Faísca, P., Trávníčková, K., Barros, A., Carobbio, S., Domingos, P.M., et al. (2023). Semaphorin 4B is an ADAM17-cleaved adipokine that inhibits adipocyte differentiation and thermogenesis. Mol. Metab. *73*, 101731. https://doi.org/10.1016/j.molmet.2023.101731.

46. Zhu, M., Wei, Y., Geißler, C., Abschlag, K., Corbalán Campos, J., Hristov, M., Möllmann, J., Lehrke, M., Karshovska, E., and Schober, A. (2017). Hyperlipidemia-induced MicroRNA-155-5p improves β-cell function by targeting Mafb. Diabetes *66*, 3072–3084. https://doi.org/10.2337/db17-0313.

47. Sweeney, S.E., Kimbler, T.B., and Firestein, G.S. (2010). Synoviocyte innate immune responses: II. pivotal role of IFN regulatory factor 3. J. Immunol. *184*, 7162–7168. https://doi.org/10.4049/jimmunol.0903944.

48. Grailer, J.J., Haggadone, M.D., Sarma, J.V., Zetoune, F.S., and Ward, P.A. (2014). Induction of M2 regulatory macrophages through the β2- Adrenergic receptor with protection during endotoxemia and acute lung injury. J. Innate Immun. *6*, 607–618. https://doi.org/10.1159/000358524.

49. Daassi, D., Hamada, M., Jeon, H., Imamura, Y., Nhu Tran, M.T., and Takahashi, S. (2016). Differential expression patterns of MafB and c-Maf in macrophages in vivo and in vitro. Biochem. Biophys. Res. Commun. *473*, 118–124. https://doi.org/10.1016/j.bbrc.2016.03.063.

50. Ağaç, D., Estrada, L.D., Maples, R., Hooper, L.V., and Farrar, J.D. (2018). The β2-adrenergic receptor controls inflammation by driving rapid IL-10 secretion. Brain Behav. Immun. *74*, 176–185. https://doi.org/10.1016/j.bbi.2018.09.004.

51. Rezaee, F., Rellick, S.L., Piedimonte, G., Akers, S.M., O'Leary, H.A., Martin, K., Craig, M.D., and Gibson, L.F. (2010). Neurotrophins regulate bone marrow stromal cell IL-6 expression through the MAPK pathway. PLoS One *5*, e9690. https://doi.org/10.1371/journal.pone.0009690.

52. Clausen, B.E., Burkhardt, C., Reith, W., Renkawitz, R., and Förster, I. (1999). Conditional gene targeting in macrophages and granulocytes using LysMcre mice. Transgenic Res. *8*, 265–277. https://doi.org/10.1023/a:1008942828960.

53. Kamitani-Kawamoto, A., Hamada, M., Moriguchi, T., Miyai, M., Saji, F., Hatamura, I., Nishikawa, K., Takayanagi, H., Hitoshi, S., Ikenaka, K., et al. (2011). MafB interacts with Gcm2 and regulates parathyroid hormone expression and parathyroid development. J. Bone Miner. Res. *26*, 2463–2472. https://doi.org/10.1002/jbmr.458.

54. Suzuki, R., Nakamura, Y., Koiwai, R., Fuseya, S., Murakami, Y., Hagiwara, K., Sato, T., Takahashi, S., and Kudo, T. (2022). Global Loss of Core 1-Derived O-Glycans in Mice Leads to High Mortality Due to Acute Kidney Failure and Gastric Ulcers. Int. J. Mol. Sci. *23*, 1273. https://doi.org/10.3390/ijms23031273.

55. Robinson, M.D., Mccarthy, D.J., and Smyth, G.K. (2010). edgeR: a Bioconductor package for differential expression analysis of digital gene expression data. Bioinformatics *26*, 139–140. https://doi.org/10.1093/bioinformatics/btp616.

56. Chen, E.Y., Tan, C.M., Kou, Y., Duan, Q., Wang, Z., Meirelles, G.V., Clark, N.R., and Ma'ayan, A. (2013). Enrichr: interactive and collaborative HTML5 gene list enrichment analysis tool. BMC Bioinf. *14*, 128. https://doi.org/10.1186/1471-2105-14-128.

57. Kuleshov, M.V., Jones, M.R., Rouillard, A.D., Fernandez, N.F., Duan, Q., Wang, Z., Koplev, S., Jenkins, S.L., Jagodnik, K.M., Lachmann, A., et al. (2016). Enrichr: a comprehensive gene set enrichment analysis web server 2016 update. Nucleic Acids Res. *44*, W90–W97. https://doi.org/10.1093/nar/gkw377.

58. Xie, Z., Bailey, A., Kuleshov, M.V., Clarke, D.J.B., Evangelista, J.E., Jenkins, S.L., Lachmann, A., Wojciechowicz, M.L., Kropiwnicki, E., Jagodnik, K.M., et al. (2021). Gene Set Knowledge Discovery with Enrichr. Current Protocols *1*. https://doi.org/10.1002/cpz1.90.

59. Yadav, M.K., Inoue, Y., Nakane-Otani, A., Tsunakawa, Y., Jeon, H., Samir, O., Teramoto, A., Kulathunga, K., Kusakabe, M., Nakamura, M., et al. (2020). Transcription factor MafB is a marker of tumor-associated macrophages in both mouse and humans. Biochem. Biophys. Res. Commun. *521*, 590–595. https://doi.org/10.1016/j.bbrc.2019.10.125.

60. Jiang, H., Ding, X., Cao, Y., Wang, H., and Zeng, W. (2017). Dense intra-adipose sympathetic arborizations are essential for cold-induced beiging of mouse white adipose tissue. Cell Metab. *26*, 686–692.e3. https://doi.org/10.1016/j.cmet.2017.08.016.

61. Kanai, M., Jeon, H., Ojima, M., Nishino, T., Usui, T., Yadav, M.K., Kulathunga, K., Morito, N., Takahashi, S., and Hamada, M. (2020). Phenotypic analysis of mice carrying human-type MAFB p.Leu239Pro mutation. Biochem. Biophys. Res. Commun. *523*, 452–457. https://doi.org/10.1016/j.bbrc.2019.12.033.

STAR★METHODS

KEY RESOURCES TABLE

REAGENT or RESOURCE	SOURCE	IDENTIFIER
Antibodies		
Anti-UCP1	Abcam, Cambridge, U.K.	Cat# ab10983; RRID:AB_2241462
Anti-tyrosine hydroxylase	Millipore Sigma, Massachusetts	Cat# AB152; RRID:AB_390204
Anti-MAC2	Cedarlane Laboratories, Burlington, Canada	Cat# Cl8942AP; RRID:AB_10060357
Anti-NGF	Abcam, Cambridge, U.K.	Cat# ab6199; RRID:AB_2152414
Alexa fluor (AF) 647 Donkey anti-rat	Abcam, Cambridge, U.K.	Cat# ab150155; RRID:AB_2813835
AF 488 Donkey anti-rabbit	Invitrogen, Waltham, Massachusetts	Cat# A-21206; RRID:AB_2535792
AF 594 Donkey anti-rabbit	Invitrogen, Waltham, Massachusetts	Cat# A-21207; RRID:AB_141637
AF 596 Chicken anti-rat	Invitrogen, Waltham, Massachusetts	Cat# A-21470; RRID:AB_2535873
AF 488 goat anti-rabbit	Invitrogen, Waltham, Massachusetts	Cat# A-11034; RRID:AB_2576217
Anti-mouse Ly-6G/Ly-6C (Gr-1)	Biolegend, San Diego, California	Cat# 108406; RRID:AB_313370
Anti-mouse CD11b-PerCp	Biolegend, San Diego, California	Cat# 101228; RRID:AB_893233
Anti-mouse CD45-PE	Biolegend, San Diego, California	Cat# 103106; RRID:AB_312971
Anti-mouse CD45-FITC	Biolegend, San Diego, California	Cat# 157214; RRID:AB_2894427
Anti-mouse CD45-BV421	Biolegend, San Diego, California	Cat# 103138; RRID:AB_2561392
Anti-mouse CD45-APC	Biolegend, San Diego, California	Cat# 157606; RRID:AB_2876537
Anti-mouse CD45-APCcy7	Biolegend, San Diego, California	Cat# 103116; RRID:AB_312981
Anti-mouse CD45-PEcy7	Biolegend, San Diego, California	Cat# 103114; RRID:AB_312979
Anti-mouse CD45-PerCp	Biolegend, San Diego, California	Cat# 103130; RRID:AB_893343
Anti-mouse Ly6G-PE	Biolegend, San Diego, California	Cat# 127608; RRID:AB_1186104
Anti-mouse F4/80 APCcy7	Biolegend, San Diego, California	Cat# 123118; RRID:AB_893489
Anti-mouse/human Mac-2 APC	Biolegend, San Diego, California	Cat# 125420; AB_2721466
Anti-mouse IL-6 Antibody - APC	Biolegend, San Diego, California	Cat# 504508; RRID:AB_10694868
APC Rat IgG1, κ Isotype Ctrl Antibody	Biolegend, San Diego, California	Cat# 400412; RRID:AB_326518
anti-IL-6Rα antibody (MR16-1)	Chugai Pharmaceutical Co., Ltd., Tokyo, Japan	NA
Rat IgG1 isotype control	Leinco Technology, St Louis, Missouri	Cat# 1–1195; RRID:AB_2894259
Zombie Violet™	Biolegend, San Diego, California	Cat# 423114
Goat Anti-Rabbit HRP (ALI3404)	Biosource International, Camarillo, California	NA
Chemicals, peptides, and recombinant proteins		
Recombinant Mouse M-CSF Protein	R&D system, Minneapolis	Cat# 416-ML-050
(−)-Norepinephrine	SIGMA Millipore,	Cat# A7257-1G
ISOGEN	Nippon Gene, Tokyo, Japan	Cat# 317–02503
Liberase	Roche, Basel, Switzerland	Cat# 5401119001
EcoR V	Takara, Shiga, Japan	Cat# 1042A
FuGENE® 6 Transfection Reagent	Promega, Madison, Wisconsin,	Cat# E2691
In-Fusion® HD Cloning Kit	Takara, Shiga, Japan	Cat# 639650
PrimeSTAR® GXL DNA Polymerase	Takara, Shiga, Japan	Cat# R050B
Critical commercial assays		
THUNDERBIRD SYBR qPCR Mix	TOYOBO, Osaka, Japan	Cat# A4251K
NextSeq500 (Illumina) for RNA Sequencing	Tsukuba University Facility	N/A
IL-6 ELISA kit	Cedarlane, Burlington, Canada	Cat# CL89136K-96
Deposited data		
GSE225421 Gene Expression Omnibus (GEO)	This paper	GSE225421

(*Continued on next page*)

Continued		
REAGENT or RESOURCE	SOURCE	IDENTIFIER
Experimental models: Cell lines		
RAW 264.7 macrophages cell lines	Manassas, Virginia	Cat# TIB-71; RRID:CVCL_0493
Experimental models: Organisms/strains		
Mafb$^{f/f}$ Transgenic mice	Generated In-House	10.1002/2211–5463.12058.
LysM-Cre Knockin Transgenic mice	The Jackson Laboratory	RRID:IMSR_JAX:004781
CAG-Cre ERT2 Transgenic mice	The Jackson Laboratory	RRID:IMSR_JAX:004682
Adipoq-Cre Transgenic mice	The Jackson Laboratory	RRID:IMSR_JAX:010803
Mafb$^{f/gfp}$	Generated In-House	https://doi.org/10.1128/MCB.00001–06
Oligonucleotides		
Primers for RT-qPCR (See Table S3)	This Paper	N/A
Cre8, 5′-CCCAGAAATGCCAGATTACG-3′	This Paper	N/A
NLSCre: 5′-CCCAAGAAGAAGAGGGTGTCC-3′	This Paper	N/A
LysM-forward 5′-CCATTATTTCACAGCAGCATTGC-3′	This Paper	N/A
LysM-rev 5′-GCTGACTCCATAGTAGCCAG-3′	This Paper	N/A
Recombinant DNA		
pGL4.10[luc2] Vector	Promega, Madison, Wisconsin,	Cat# E665A
Dual-Luciferase® Reporter Assay System	Promega, Madison, Wisconsin,	Cat# E1910
pRL Renilla Luciferase Control Reporter Vectors	Promega, Madison, Wisconsin,	Cat# E2231
MAFB overexpressing vector	Generated In-House	https://doi.org/10.1128/MCB.00001-06
Software and algorithms		
STAR version = STAR_2.6.1a_08-27	https://github.com/	N/A
R-Programming Language (For RNA seq Analysis)	https://www.r-project.org/	N/A
Enrichr tool	https://maayanlab.cloud/Enrichr/	N/A
Partek® Flow® software version 10.0.22.1111	https://www.partek.com/partek-flow/	N/A
BZ-X810 analyzer software	Keyence Corporation, Osaka, Japan	BZ-X810
ImageJ	http://imagej.net	N/A
CytExpert software 2.4	Beckman coulter, Brea, California	2.4
Qiagen Ingeunity Pathway Analysis	QIAGEN, Redwood City, California	Version 107193442
Cytoflex flow cytometer	Beckman coulter, Brea, California	V2-B5-R3
CytExpert software 2.4	Beckman coulter, Brea, California	2.4
Other		
Rodent Rectal thermistor	skSATO, Tokyo, Japan	Cat# SK-1260
IR camera compact pro	Seek thermal, Inc. Santa Barbara, USA	N/A
Mlx90614ESF IR-Sensor	Melexis, Ypres, Belgium	Cat# Mlx90614ESF
Indirect calorimeter for mice	Muromachi Kikai Co., Ltd., Tokyo, Japan	Cat# MK-5000RQ
Keyence BZ-X 810 fluorescence microscope	Keyence Corporation, Osaka, Japan	BZ-X 810
Ultra microscope II	Miltenyi Biotec, Bergisch Gladbach, Germany	N/A
iBright Imaging Systems	Thermofisher Scientific, Waltham, Massachusetts	N/A

RESOURCE AVAILABILITY

Lead contact

Michito Hamada, Ph.D., Department of Anatomy and Embryology, Faculty of Medicine, University of Tsukuba, 1-1-1 Tennodai, Tsukuba 305-8575, Japan; Phone: +81-298-53-7516, Fax: +81-298-53-6965, E-mail: hamamichi@md.tsukuba.ac.jp (Lead Contact)

Materials availability

This study did not generate new unique reagents.

Data and code availability

- RNA sequencing data generated for this study is submitted to Gene Expression Omnibus (GEO), under the accession number GSE225421 (https://www.ncbi.nlm.nih.gov/geo/query/acc.cgi?acc=GSE225421).
- This study did not generate any original code.
- Any other data presented in this manuscript can be obtained by contacting the lead author upon request.

EXPERIMENTAL MODEL AND STUDY PARTICIPANT DETAILS

Animals

Macrophage-specific *Mafb*-deficient mice (*Mafb*$^{f/f}$*::*LysM-Cre) were generated by mating *Mafb*$^{f/f}$ and LysM-Cre Knockin to obtain *Mafb*$^{f/f}$:LysM-*Cre* mice. The *Mafb*$^{f/f}$ and LysM-Cre Knockin mice were created in our laboratory as previously described.[16,52] Mice were shifted from light to dark phase at 19:00 and 05:00. The genotypes were detected by PCR using tail tissue DNA with the following primer sequences: Cre8, 5′-CCCAGAAATGCCAGATTACG-3′; NLSCre: 5′-CCCAAGAAGAAGAGGGTGTCC-3′; LysM-forward 5′-CCATTATTTCACAGCAGCATTGC-3′; and LysM-rev 5′-GCTGACTCCATAGTAGCCAG-3′. *Mafb*$^{f/f}$*::*CAG-Cre ERT2 generated by *Mafb*$^{f/f}$ crossing with CAG-Cre ERT2 transgenic mice (The Jackson Laboratory, Bar Harbor, ME, USA) to obtain *Mafb*$^{f/f}$:CAG-Cre ERT2 mice.[53] The Cre recombinase had been fused to a mutated ligand binding domain of the human estrogen receptor (ER), resulting in a tamoxifen-dependent Cre recombinase, Cre-ER(T), that is activated by tamoxifen, but not by estradiol. After the injection of tamoxifen at 8 weeks of age, we obtained MAFB tamoxifen-inducible global KO mice. *Mafb*$^{f/f}$*::*Adipoq-Cre was generated by crossing *Mafb*$^{f/f}$ with Adipoq-Cre transgenic mice (The Jackson Laboratory).[54] *Mafb*$^{+/gfp}$ animals were created in our laboratory as previously described.[13] Wild-type C57BL/6J mice were purchased from SLC. We used only age- and weight-matched 8–12-week-old mice for our experiments. All mice were maintained under specific pathogen-free conditions, in controlled temperature, humidity, food access, and water access environment, and with minimum and maximum mice per cage defined as per relevant Japanese institutional Regulations and guidelines at the Laboratory Animal Resource Center of the University of Tsukuba. All animal experiments were performed in compliance with the relevant Japanese institutional laws and guidelines and have been approved by the University of Tsukuba Animal Ethics Committee.

METHOD DETAILS

Cold exposure experiments

The protocol for mouse cold exposure experiments was pre-approved by the University of Tsukuba Animal Ethics Committee. An acute cold exposure study for 4–8 h at 8°C was performed after intermittent cold exposure on alternate days at 8°C for up to 8 h for habituation. The 24-h cold exposure experiments were conducted by slowly decreasing temperatures to 4°C (first 2h 12°C, 8°C for 2h, and then 4°C for the remaining 20h. Continuous cold exposure experiments were performed for 10 days with slight modifications from the previously published protocol of Murano et al.[2] Mice were subjected to cold exposure for 10 days with three days of gradually decreasing temperature to 4°C (first day at 12°C, second day at 8°C, day 3–10 at 4°C).

Bone marrow-derived macrophage culture

BMDM was cultured as previously described.[15] Mice were euthanized, and the bone marrow from both hind paws was collected under sterile conditions. After RBC lysis, 1 × 10^7 per 10 mL of cells cultured in Dulbecco's modified Eagle medium (DMEM) containing 10% fetal bovine serum (FBS; FB-1380, Biosera, Nuaille, France), 1% MEM-NEAA (MEM-NEAA; 11140050, GIBCO; Thermo Scientific INC, Massachusetts), 1% penicillin-streptomycin (15140122, GIBCO), 2 mM L-glutamine (25030081, GIBCO), 0.05 mM beta-mercaptoethanol (133–14571, Fujifilm Wako, Osaka, Japan), and M-CSF 10 ng/mL/day (416-ML-050, R&D system, Minneapolis). On day three, non-adherent cells were removed, and adherent cells were detached using Accutase (A1110501, GIBCO), then washed, counted, and cultured for another three days. Norepinephrine (NE) treatments for 500nM, 1000nM, & 5000nM were performed 12 h before experiments.

Peritoneal macrophage culture

Peritoneal macrophages were cultured as previously described.[15] We injected thioglycolate into the abdominal cavities of the mice, and after four days, mice peritoneal cells were collected. Cells were plated at 5 × 10^5–1×10^6 cells per 4 mL in a 6 cm dish using media described in the BMDM culture. NE treatments for 500nM, 1000nM, & 5000nM/100 ng LPS treatment were performed 2–24 h before experiments.

RT-qPCR

The total RNA of desired tissue or cells was extracted using ISOGEN (Nippon Gene, Tokyo, Japan). cDNA was synthesized using a QuantiTect Reverse Transcription Kit (Qiagen, Hilden, Germany). RT-qPCR was used to examine the desired mRNA levels on a Thermal Cycler Dice Real-Time System (Takara Bio, Shiga, Japan) using THUNDERBIRD SYBR qPCR Mix (TOYOBO, Osaka, Japan). mRNA abundance was normalized to that of mouse *36b4* mRNA. The specific primer sequences used are listed in Table S3.

Measurement of rectal and skin temperature

The rectal temperature in mice was measured with a thermistor (SK-1260, skSATO, Tokyo, Japan) lubricated and inserted 2 cm deep. Skin temperature was assessed using an IR camera compact pro (Seek thermal, Inc. Santa Barbara, USA).

Intracapsular BAT temperature recording

Mlx90614ESF (Melexis, Ypres, Belgium) medically calibrated IR sensors were programmed using the Adfruit GitHub online libraries to read on the Aurdino device. A Python program was written to handle multiple devices initiating and reading their data in an Excel file. The sensor was attached to the mouse skin using a 3D-printed adapter and skin glue. The system was designed such that the mice could freely move as the sensor was attached to a freely rotating pulley circuit with an ultrathin wire. Intracapsular temperature was recorded using this self-made device for up to 4 h.

Relative VO_2 measurement

Metabolic parameters were measured using an indirect calorimeter (MK-5000RQ; Muromachi Kikai Co., Ltd., Tokyo, Japan) under cold conditions and after administering CL316243, a β3 agonist drug (ab144605, Abcam, Cambridge, U.K.), to compare BAT function between *Mafb*$^{f/f}$ and *Mafb*$^{f/f}$*::*LysM-Cre mice. The instrument outputs were VO_2 [mL/min], VCO_2 [mL/min], and RQ; we converted absolute VO_2 [mL/min] into relative VO_2 [mL/kg/min].

RNA sequencing

RNA was processed using Qiagen RNeasy Plus Universal Mini Kit. RNA quality control and library preparation from 500 ng of RNA and paired-end RNA sequencing using NextSeq500 (Illumina) were performed by a sequencing facility service at Tsukuba University. Raw data were aligned and mapped to the mouse reference genome mm-10 using STAR_2.6.1a_08–27 default parameters, followed by feature count. The RNA sequencing data were analyzed by empirical analysis of differential gene (edgeR) package of R software,[55] and differentially expressed genes ($p < 0.05$ and $q < 0.2$) were analyzed using an online Enrichr tool for KEGG Pathway, WikiPathway, GO Molecular Function, and Mouse Gene Atlas.[56–58] Sequencing data were deposited in the NCBI GEO public database GSE225421.

Single cell RNA sequencing analysis

Single-cell RNA sequencing data of iBAT SVF sorted into lineage positive and negative was downloaded from GSE207706 and analyzed using Partek Flow software version 10.0.22.1111Data ref. [21]. QA/QC were used to remove dead cells, empty reads, duplets, and batch differences. Data were normalized and processed with PCA, graph-based clustering, and tSNE plot. Biomarkers were identified for cell populations, and Enrichr tools were used for cell population definition using various databases such as Mouse Gene Atlas, Azimuth Cell Types 2021, PanglaoDB Augmented 2021, CellMarker Augmented 2021, and Tabula Muris.[56–58]

Immunohistochemistry (IHC)

Brown adipose tissues were fixed, dehydrated, paraffin-embedded, sectioned, and deparaffinized. Antigens were retrieved using TE buffer (pH 9.0) by autoclaving for 2–10 min at 110°C with slow cooling. Non-specific blocking was performed using 10% serum, including 1% bovine serum albumin (BSA), 3% skimmed milk, 0.02% sodium azide, and 0.1% Triton X-100. Primary antibodies were incubated for 2–3 h at room temperature or for 8–48 h at 4°C in the blocking buffer. The secondary antibody was incubated for 1 h at room temperature. The slides were washed and mounted in Fluoromount^{Tm} (Diagnostic Biosystem, California) media. Nuclei were stained with Hoechst (2 μg/mL, 1368-F, Diagnostic Biosystem). Images were acquired using a Keyence BZ-X 810 fluorescence microscope, analyzed, and quantified using BZ-X810 analyzer software as described previously or ImageJ (Fiji).[59] The list of primary and secondary antibodies is provided in (Key resource table).

3DISCO staining and imaging

Following the 3DISCO protocol established by Jiang et al. for adipose tissue,[60] mice iBAT was collected after perfusion with PBS containing 10 μg/mL of heparin. Blocking for non-specific binding was performed using donkey serum and Fc-block for 24 h. Anti-tyrosine hydroxylase staining for SN was performed for 72 h, followed by washing and secondary antibody incubation for 48 h (Appendix Table S4). The tissue was washed for 10 h, mounted in agarose, and a delipidation step was performed for 72 h at 4°C. The agarose block was cleared by using dibenzyl ether (Fujifilm Wako, Osaka, Japan) and sent to Miltenyi Biotec, Tokyo, for volume imaging using an ultra microscope II. Volume imaging was optimized, and full 3-D images were provided for comparison.

Hematoxylin and eosin (HE) staining

HE staining was done as previously described,[61] with optimization for BAT. Paraffin sections of 5 μm thickness were deparaffinized, and Mayer's hematoxylin (131–09665, Fujifilm Wako, Osaka, Japan) staining was performed for 20 min. Sections were washed in flowing tap water for 1 min and differentiated using a differentiation solution (A3179, Sigma) for 30 s. Sections were washed serially in tap water for 5 min and 2 min in Scott tap water (S5134, Sigma-Aldrich, Missouri) and again for 1 min in tap water. Sections were dehydrated using ethanol 95–100% for 5 min each and stained with eosin (050–06041, Fujifilm Wako, Osaka, Japan) for 2 min.

Sections were washed in ethanol, cleaned with xylene, and mounted using D.P.X. (317616, Sigma-Aldrich, Missouri). Images were acquired using a Keyence BZ-X 810 fluorescence microscope, analyzed, and quantified using BZ-X810 analyzer software as described previously.[59]

IL-6 cytokine ELISA

Tissue lysates were prepared in RIPA buffer, and IL-6 concentration was measured using a Cedarlane CL89136K-96 ELISA kit, following the manufacturer's protocol. Detection was performed at 450 nm using a plate reader.

Western blot

One-half of the complete iBAT of mice that underwent cold exposure was lysed in RIPA buffer containing complete protease inhibitor cocktail (Roche). The protein lysate was measured using the BCA assay, and 20μg of total protein was loaded into SDS page. After running and transferring the gel onto a PVDF membrane, blocking and staining for primary antibody for NGF and secondary antibody conjugated with HRP were performed. Signals were developed using Immobilon western chemiluminescent horseradish peroxidase substrate (Millipore) and visualized using the iBright imaging system (Thermo Fisher Scientific). The primary antibody was rabbit anti-mouse/human NGF (ab6199, abcam), and the secondary antibody was goat anti-rabbit HRP (Biosource International).

Isolation of BAT SVF

BAT SVF was isolated through enzymatic digestion using Liberase (5401119001, Roche, Basel, Switzerland). iBATs were minced and digested in Hanks' balanced salt solution containing Liberase 0.5 U/mL, 2% FBS, and 10 mM 2-[4-(2-hydroxyethyl)piperazin-1-yl] ethanesulfonic acid by incubating in a shaker with 150 rpm speed at 37°C. The reaction was stopped by adding 10 volumes of PBS containing 0.5% BSA and filtered using a 70 μm filter. The filtrate was centrifuged at 300 × *g* for 5 min, and the pellet was washed using PBS containing 0.5% BSA, followed by RBC lysis using an ammonium-chloride-potassium (ACK) lysis buffer. After the final wash, cells were counted and used for cytometry or RNA analysis.

Flow cytometry and intracellular IL-6 staining

SVF of iBAT of mice was collected as described above and stained for Zombie Violet^{Tm} (423114, Biolegend, California) for 15 min, followed by surface antibodies for 20 min at 4°C. The cells were fixed with 5 N formalin in PBS, permeabilized using 0.1% saponin, stained for 20 min, washed twice with 0.1% saponin, and analyzed using Cytoflex (Beckman Coulter Life Sciences, Indianapolis) with CytExpert software 2.4. Gating is shown in Appendix Figure S6. For intracellular staining of IL-6, mice were injected 250 μg of Brefeldin A (420601, Biolegend, California) 6 h before the experiment, and all reagents for SVF isolation and staining were included in Brefeldin A 1x injection.

Luciferase reporter assays

IL-6 promoter region up to 1153BP upstream of the transcription start site of IL-6 was amplified from C57BL6/J mice genomic DNA using PrimeStar GXL (Takara). The PCR product was ligated into the EcoRV site of the promoter-less luciferase Luc2 vector (pGL4.10, Promega) using In-Fusion HD cloning Kit (Takara). This promoter region contained two MAFB binding sites: 3'–AGTT**TG ACCCA**GCCTA–5′, and 3′—AGTG**CTGAGT**CACTTT—5′, Zhu M. et al. reported and demonstrated in the MIN6 cell line that MAFB binding to this region led to suppression of IL-6 expression.[24] To examine whether MAFB could suppress the IL-6 promoters in macrophages, the IL-6 luciferase vector was co-transfected with the MAFB-expressing vector into RAW264.7 cells at 0 ng and 50 ng concentrations. The transfection was performed using FuGENE6 transfection reagent (Promega). The cells were then cultured for 12 or 24 h, with or without 100 ng of LPS treatment. The luciferase assay was performed with the Dual-Luciferase Reporter Assay System (Promega). Briefly, after transfection for 12 or 24 h, the cells were lysed, and 20 μL of cell lysate was transferred to 100 μL of Luciferase Assay Reagent II (LARII). The samples were then measured using a luminometer. A 100-μL quantity of Stop&Glo reagent was added to the samples, and they were again measured. The pRL-TK (Promega)-expressing vector was co-transfected into RAW264.7 cells. A pRL-TK vector expressing *Renilla reniformis* luciferase was used to normalize the transfection efficiency.[15] The results were further normalized with an empty vector.

Anti-IL-6Rα rescue experiments

A 200 μg loading dose of anti-IL-6Rα antibody (MR16-1, Chugai Pharmaceutical Co., Ltd., Tokyo, Japan) was injected intraperitoneally before cold exposure, with a 50 μg maintenance dose after seven days, while an equivalent amount of Rat IgG1 isotype control (1–1195, Leinco Technology, St Louis, Missouri) or PBS was used as control. For the 24-h cold experiment, the loading dose was given eight days earlier, and the maintenance dose a day before starting the experiment.

QUANTIFICATION AND STATISTICAL ANALYSIS

Data are presented as the mean ± SEM of at least two independent experiments. We used Prism10.1.0 software for our statistical calculation. The relevant statistical analysis for individual plots is mentioned in the figure legends. Results for each statistical test with p value <0.05 were considered significant.